International Journal of Earth Sciences
https://doi.org/10.1007/s00531-024-02433-7

ORIGINAL PAPER

Latest Pliensbachian to Early Toarcian depositional environment and organo-facies evolution in the North-German Basin (Hondelage Section)

Tim Marten[1] · Wolfgang Ruebsam[1] · Jörg Mutterlose[2] · Guido L. B. Wiesenberg[3] · Lorenz Schwark[1,4]

Received: 3 April 2024 / Accepted: 31 May 2024

Abstract

The Pliensbachian/Toarcian boundary interval represents a transition from a coldhouse into a hothouse climate state, involving the demise of a land-based cryosphere, initiating a third-order global sea-level rise. Within the intensely studied Northwest Tethyan shelf region, the South-German Basin has been investigated in more detail than the North-German Basin (NGB). We here provide a palaeoenvironmental reconstruction of the Pliensbachian/Toarcian transition from the Hondelage fossil excavation site located in the NGB employing organic, isotope, and major/trace element proxies. Here, the late Pliensbachian was characterized by cold climate, low sea level, and a slow hydrological cycle, causing minor terrigenous sediment and nutrient fluxes to the basin, instigating low marine productivity. Shallow, well-mixed shelf waters of normal salinity favored aerobic degradation of planktonic biomass, preventing sedimentary accumulation of organic matter. These conditions changed in the earliest Toarcian, where increased temperatures led to sea-level rise via meltdown of land-based ice and accelerated the hydrological cycle, causing salinity stratification. Enhanced riverine sediment and nutrient supply from nearby landmasses promoted marine primary productivity, which caused anoxic conditions in bottom and pore waters favoring enhanced preservation and accumulation of organic matter. A short-lived sea-level fall at the Lower Elegans Bed coincided with lowered productivity and enhanced carbonate precipitation, due to reduced runoff and recovery of the carbonate factory. Increased redox-sensitive trace element concentrations above the Lower Elegans Bed suggest a renewed inflow of low-salinity arctic water masses via the Viking Corridor and potentially increased freshwater input, promoting water column stratification, enhanced planktonic productivity, and re-establishment of bottom water anoxia/euxinia.

Keywords Redox assessment · Organic matter preservation · Toarcian Oceanic Anoxic Event · Global warming · Toarcian sea level

Introduction

The latest Pliensbachian to early Toarcian was characterized by major climate swings that were paralleled by rapid high-amplitude sea-level cycles (Fig. 1) (e.g., Morard et al. 2003; Suan et al. 2010; Pittet et al. 2014; Korte et al. 2015; Krencker et al. 2019; Ruebsam et al. 2020a). Climate and sea-level dynamics have been related to orbitally forced glacial–interglacial cycles, which is supported by the occurrence of glacial deposits in strata of latest Pliensbachian age (e.g., Kaplan 1978; Suan et al. 2011; Teichert and Luppold 2013; Ruebsam and Schwark 2021; Merkel and Munnecke 2023). Latest Pliensbachian to early Toarcian environmental instabilities affected marine and continental ecosystems (e.g., Little and Benton 1995; Harries and Little 1999; Mattioli et al. 2008; Danise et al. 2015; Slater et al. 2019), as

✉ Tim Marten
tim.marten@ifg.uni-kiel.de

✉ Lorenz Schwark
lorenz.schwark@ifg.uni-kiel.de

[1] Department of Organic and Isotope Geochemistry, Institute of Geoscience, University of Kiel, 24118 Kiel, Germany

[2] Institute for Geology, Mineralogy and Geophysics, Ruhr-University Bochum, 44801 Bochum, Germany

[3] Department of Geography, University of Zurich, 8057 Zurich, Switzerland

[4] Department of Earth and Planetary Sciences, WA-OIGC, Curtin University, Bentley, Perth 6102, Australia

Published online: 27 June 2024

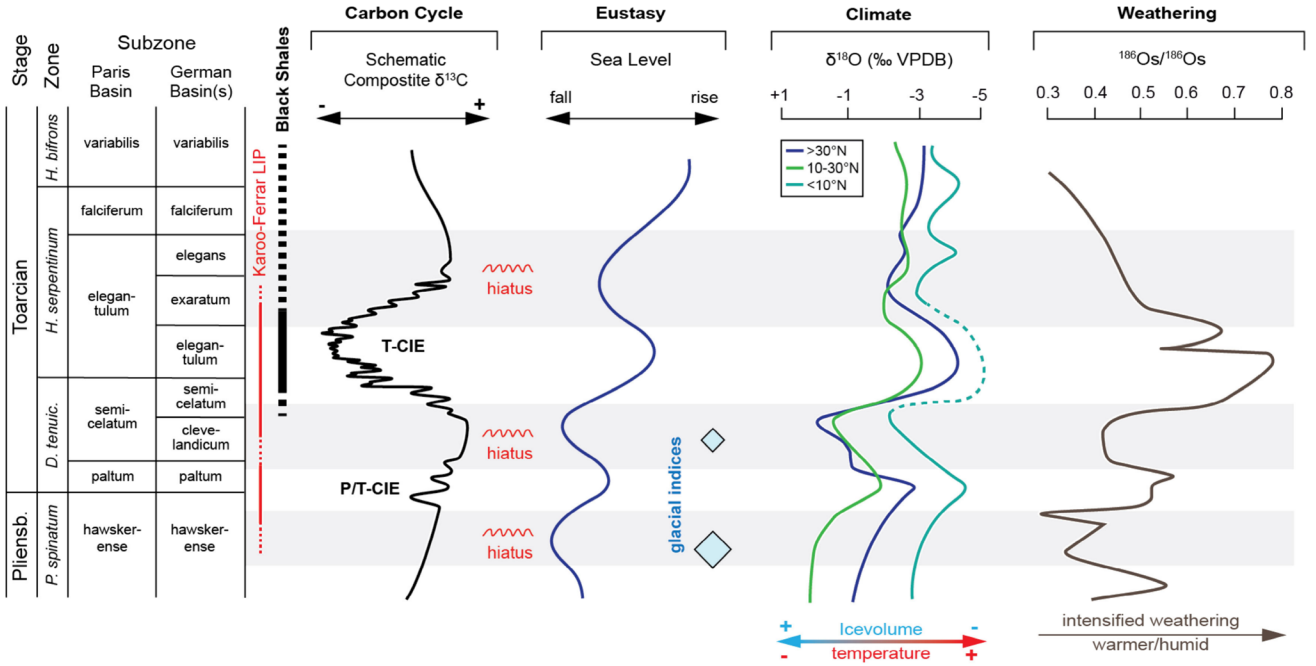

Fig. 1 Generalized evolution of carbon cycle (P/T-CIE: Pliensbachian/Toarcian carbon isotope excursion; T-CIE: Toarcian carbon isotope excursion), eustatic sea level, climate and weathering during the latest Pliensbachian and early Toarcian in the EEBS (European Epicontinental Basin System) (modified from Ruebsam et al. 2020b). The T-CIE coincides with the onset of widespread black shale deposition at shelf seas. Early Toarcian environmental change was potentially triggered by the emplacement of the Karoo-Ferrar Large Igneous Province (LIP) shown by a thin red line. Ammonite zonation schemes for the German and Paris basins are after Page (2003). The thick black line marks intervals of global black shale deposition, the stippled line indicates regional black shale deposition (Ruebsam and Schwark 2024)

well as depositional conditions at shallow shelf areas. In particular, high-amplitude sea-level changes resulted in recurrent erosive events and stratigraphic condensation (e.g., Morard et al. 2003; Krencker et al. 2019; Ruebsam et al. 2019; Ruebsam and Al-Husseini 2020; Bodin et al. 2023).

Climate fluctuations culminated in an early Toarcian greenhouse that reconciles the genesis of the Toarcian Oceanic Anoxic Event (T-OAE Fig. 1), also termed "Jenkyns Event" (Müller et al. 2017; Gambacorta et al., 2023), a major organic carbon burial event of trans-regional, potentially global extent (Jenkyns 1988, 2010; Kemp et al. 2022). Deposition of organic carbon (OC)-rich strata (black shales, sensu lato) was most extensive across the northern part of the northwest Tethys shelf, an intensively structured shallow shelf area (Ziegler 1990), where black shale deposition was promoted by the interplay of local, regional, and global factors. These include seal-level changes, hydrological cycling, hydrological restriction, surface water freshening, freshwater stratification, and substantial nutrient supply via increased riverine discharge (e.g., Jenkyns 1988, 2010; Saelen et al. 1996; Cohen et al. 2004; Hermoso et al. 2013).

Warming phases at the Pliensbachian/Toarcian boundary interval and in the early Toarcian (Tenuicostatum–Serpentinum zonal boundary interval) were accompanied by perturbations of the global carbon cycle (Fig. 1) that manifested in negative carbon isotope excursions, i.e., Pliensbachian/Toarcian Carbon Isotope Excursion: P/T-CIE and Toarcian Carbon Isotope Excursion: T-CIE (Hesselbo et al. 2000, 2007; Kemp et al. 2005; Suan et al. 2011; for a review see Ruebsam and Al-Husseini 2020). Although frequently used as synonyms, the T-CIE and the T-OAE show a disparity depending on regional conditions of sedimentation (Ruebsam and Schwark 2024). Carbon cycle perturbations were related to recurrent events of ^{12}C-enriched carbon release (Beerling and Brentnall 2007). The potential carbon sources discussed include emissions from gas hydrates, wetlands, cryosphere (Hesselbo et al. 2000; Kemp et al. 2005; Them et al. 2017; Ruebsam et al. 2019) as well as volcanic processes, including intrusions into organic rich strata associated with thermogenic methane release, linked to the emplacement of the Karoo-Ferrar Large Igneous Province (K-F-LIP) in southern Gondwana (e.g., Svensen et al. 2007; Percival et al. 2015).

The response of depositional environments and marine ecosystems to late Pliensbachian to early Toarcian environmental change has been extensively studied from sediment successions in North Africa (e.g., Reolid et al. 2012, 2013; Baghli et al. 2022; Krencker et al. 2022; Ruebsam et al.

2022a), the Mediterranean realm (e.g., Jenkyns 1988; Mattioli and Pittet 2002, 2004; Reolid et al. 2018; Ruebsam et al. 2020a; Visentin and Erba 2021), the Paris Basin (e.g., van Breugel et al. 2006; Hermoso et al. 2009, 2013; Ruebsam et al. 2022b), the South-German Basin (Prauss et al. 1991; Röhl et al. 2001; Frimmel et al. 2004; Schwark and Frimmel 2004; Montero-Serrano et al. 2015; Ajuaba et al. 2022), and the British Islands (e.g., Jenkyns and Clayton 1986, 1997; McArthur et al. 2008; Xu et al. 2018). Detailed and stratigraphically well-constrained data from the central area of the NGB are, however, relatively rare. Pioneer work (Wunnenberg 1927; Hoffmann 1966, 1968; Riegel et al. 1986; Loh et al. 1986; Brumsack 1991; Prauss 1996) provided detailed palynological, geochemical, and sedimentological information, but lacked a detailed stratigraphic context. Furthermore, several studies focusing on maturity and source rock potential have been conducted on Posidonia Shale from the Hils syncline (Rullkötter et al. 1988; Littke et al. 1991a, b; Song et al. 2017; Stock et al. 2017). Recently, studies from the NGB (van de Schootbrugge et al. 2019; Mutterlose et al. 2022; Visentin et al. 2022; Burnaz et al. 2024; Ruebsam et al. 2024) presented sedimentological, palaeontological, and geochemical data embedded in a robust bio- and chemostratigraphic framework.

In this study, we investigate the latest Pliensbachian to early Toarcian strata of the stratigraphically well-defined Hondelage succession of the NGB (Fig. 2). Whereas previous work (Mutterlose et al. 2022) documented the ecological response of nannofossils and marine invertebrates, we here present inorganic, bulk organic and isotope geochemical data to assess changes in depositional conditions and organo-facies in response to latest Pliensbachian to early Toarcian environmental changes. In particular, this study aims to improve the understanding of Toarcian environmental variations in the NGB, where they have been insufficiently studied.

Geological setting and stratigraphy

The NGB was part of the European Epicontinental Basin System (EEBS), a large epicontinental sea in the northern part of the Northwest Tethyan Shelf. The EEBS was intensively structured into several basins, such as the Paris Basin, the Lorraine Basin, the South-German Basin, the North-German Basin, the Dutch basins, or the British basins. These basins were separated by shoals, swells, and islands of variable size (Ziegler 1990). The EEBS was connected to the Arctic Ocean through the Viking Corridor (Fig. 2). South of the EEBS the North-West Tethys Shelf opened to the Tethys toward the southeast. Water-mass exchange between the Tethys Ocean and open North-West Tethyan Shelf with the EEBS was limited by numerous islands and swells, which varied in size depending on eustatic sea-level fluctuations (Ziegler 1990).

The current study site, the Hondelage pit, a Fossillagerstätte famous for its rich fossil inventory is located 1 km north of the village Hondelage, near Braunschweig (Germany). The pit is currently mined for fossils by the Natural History Museum Braunschweig. Throughout the last 20 years, the section has provided rich fossil material of a marine ecosystem. The entire suite from single celled primary producers, via rich mollusc assemblages (bivalves, belemnites, gastropods, ammonites) up to fishes and ichtyosaurs has been recovered (Klopschar 2006; Mutterlose et al. 2022). As such, Hondelage offers an ideal opportunity to understand not only the paeloenvironmental evolution of the Pliensbachian–Toarcian but also the response of the marine fauna. In the Early Jurassic, the study site was located in the south-eastern part of the NGB at a palaeolatitude ~ 45°N (van Hinsbergen et al. 2015) within a local depression, the Oberaller Through (Fig. 2b). This depression was bordered by the Calvörde Island and Altmark Swell to the north, and by the Fallstein Swell to the south (Ruebsam et al. 2024). Regional factors, such as halotectonically induced uplift, most probably caused a formation of small-scaled basins and swells. To the east, in proximity to the Bohemian Massif, a shallow marine depositional setting is indicated by a more sandy facies (Ott 1967).

The Hondelage succession is mainly composed of claystones and calcareous claystones of latest Pliensbachian (Amaltheenton Formation) to lower Toarcian age (Posidonia Shale Formation) (Fig. 2c). For the Hondelage outcrop, a detailed biostratigraphic framework is based on ammonites and calcareous nannofossils (Mutterlose et al. 2022). As the Amaltheenton Formation lacks diagnostic ammonites, a late Pliensbachian age was inferred from the calcareous nannofossil *Crepidolithus impontus* that is characteristic for the late Pliensbachian Nannofossil Zone NJ5b (Mutterlose et al. 2022). The Posidonia Shale Formation contains a rich marine flora and fauna including calcareous nannofossils, ammonites, fishes, and marine reptiles. Ammonite findings allow to differentiate the *semicelatum* Subzone of the *D. tenuicostatum* Zone, as well as the *elegantulum*, *exaratum,* and *elegans* subzones of the overlying *H. serpentinum* Zone. Calcareous nannofossil assemblages further allow to assign the Posidonia Shale Formation to the Nannofossil Zone NJ6 (Mutterlose et al. 2022). The calcareous nannofossil calcification crises, recorded from the nearby Schandelah core (Visentin et al. 2022), is not well expressed in Hondelage due to the hiatus at the base of the Toarcian. Nevertheless, the onset of a nannofossil bloom slightly postdates the onset of the negative T-CIE (Mutterlose et al. 2022). The $\delta^{13}C_{org}$ data show a negative carbon isotope excursion in strata corresponding to the upper *D. tenuicostatum* and the lower *H. serpentinum* zones (Mutterlose et al. 2022). This

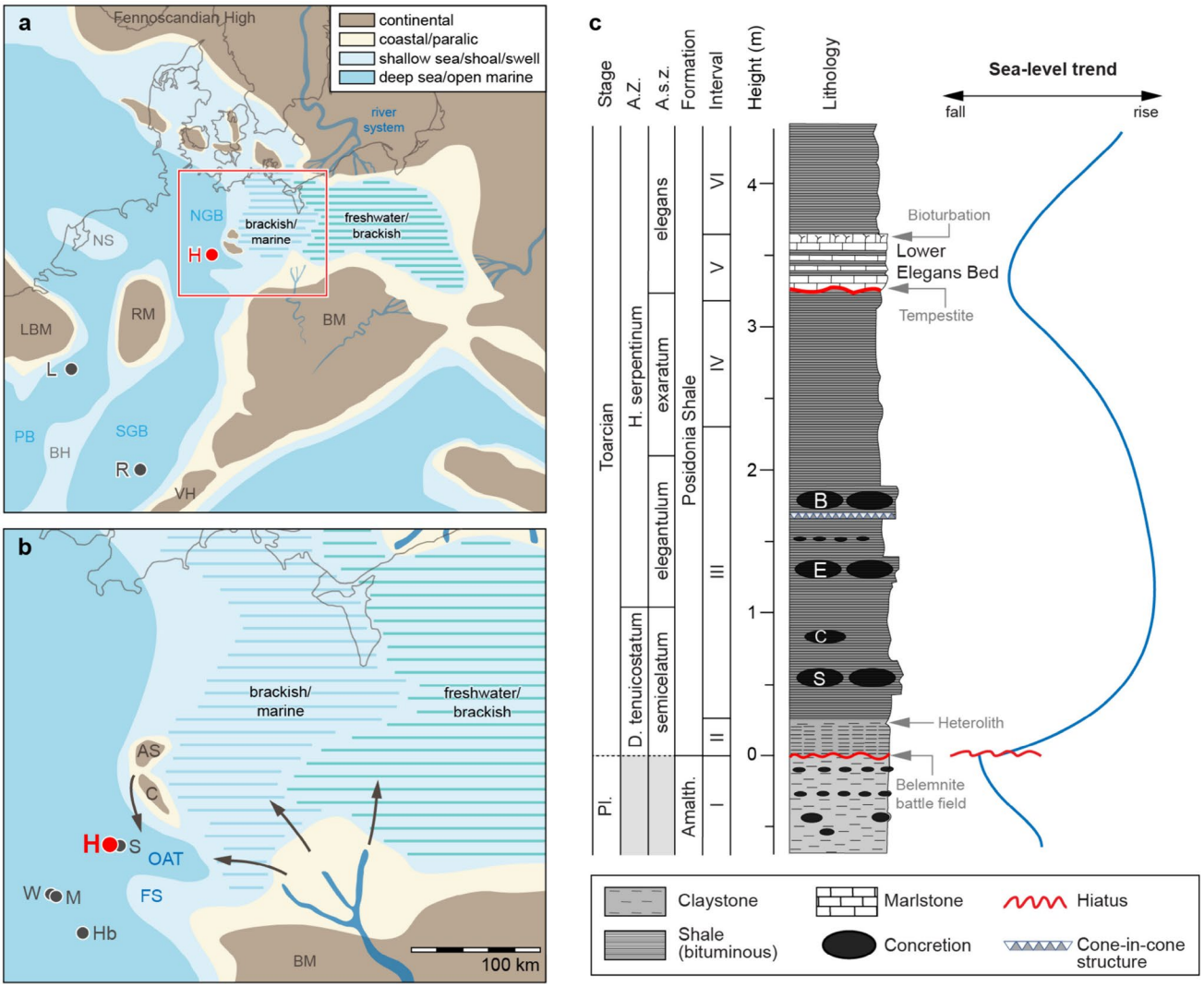

Fig. 2 **a**: Palaeogeographic map of the Early Toarcian in northern Europe, showing the study site (*H* Hondelage) and localities mentioned in the text (*R* Rietheim and L Luxemburg) (*BM* Bohemian Massif, *RM* Rhenish Massif, *LBM* London Brabant Massif, *VH* Vindelician High, *PB* Paris Basin, *SGB* South-German Basin, *NGB* North-German Basin). The palaeogeographic map is modified from Ziegler (1990), Barth et al. (2018), and Ruebsam et al. (2020c, 2024). **b:** Detailed palaeogeographic reconstruction of the study area, the south-eastern North-German Basin. Localities mentioned in the text are: S: Schandelah, W: Wickensen, M: Mainzholzen, and Hb: Hainberg. Regional palaeogeographic elements, such as the Oberaller Trough (OAT), the Calvörde Island (C), the Altmark Swell (AS), and the Fallstein Swell (FS) are indicated. Sediment supply (arrows) was sourced from small islands in the north and from the Bohemian Massif (BM) in the southeast (Zimmermann et al. 2018; Barth et al. 2018; Ruebsam et al. 2024; Ott 1967). **c:** Lithostratigraphic column with ammonite biostratigraphy (Mutterlose et al. 2022) and simplified sea-level trend (Hallam 1997; Morard et al. 2003; Wignall 2005; Ruebsam and Al-Husseini 2021). A. Z.: Ammonite Zone; A. s.z.: Ammonite subzone; Interval I: Pliensbachian; Interval II: basal Posidonia Shale Formation; Interval III: T-CIE; Interval IV: post-CIE; Interval V: Lower Elegans Bed; Interval VI: upper Posidonia Shale Formation. S: siemensi concretion layer; C: capillatum concretion layer; E: elegantulum concretion layer B: borealis concretion layer

characteristic chemostratigraphic feature has been interpreted to reflect the T-CIE, which has been reported from coeval strata worldwide and acts as important chemostratigraphic marker (e.g., Hesselbo et al. 2000, 2007; Röhl et al. 2001; Kemp et al. 2005; Suan et al. 2011; Them et al. 2017; for a review see Ruebsam and Al-Husseini 2020).

Biostratigraphy and carbon isotope-based chemostratigraphy indicate a hiatus at the Pliensbachian/Toarcian boundary. In particular, most of the lower part of the *D. tenuicostatum* zone, including the *semicelatum, tenuicostatum, clevelandicum, crosbeyi,* and *paltum* biohorizons, as well as the Pliensbachian/Toarcian boundary interval appear to be absent. The upper part of the *D. tenuicostatum* Zone rests unconformably on the underlying Amaltheenton Formation of the Pliensbachian. At comparable stratigraphic intervals, pronounced hiatuses of variable duration have

been reported from numerous sites and most likely resulted from erosive events during a major sea-level lowstand (e.g., Jenkyns 1985; Riegel et al. 1986; Hallam 1997; Morard et al. 2003; Wignall 2005; van Breugel et al. 2006; Suan et al. 2011; Ruebsam and Al-Husseini 2020). At Hondelage, this hiatus/erosive horizon is marked by the "Belemnite Battlefield", a distinctive bed enriched in belemnites that have been corroded (Mutterlose et al. 2022). In addition, the erosive/reworked base at the Lower Elegans Bed (Fig. 2c) suggests deposition by a tempestite pointing toward a lowered sea level. Stratigraphic gaps, resulting from erosive events occurring in the same stratigraphic interval, have been described from several sections (e.g., Thibault et al. 2018; Ruebsam and Al-Husseini 2020).

Methods

Sample preparation

In total, 109 samples were collected at the Hondelage outcrop, covering uppermost Pliensbachian to lower Toarcian strata, covering ~ 3 Ma. The Pliensbachian Amaltheenton Formation is represented by 16 samples and the Toarcian Posidonia Shale Formation by 93 samples. To minimize the impact of contamination, rock surfaces were removed using sandpaper. Cleaned samples were crushed and powdered using a mortar. Afterward, samples were dried at ~ 40 °C for 48 h to remove residual moisture.

CNS analysis

The original sample material was analyzed for its total nitrogen (TN), total sulfur (TS), and total carbon (TC) contents using an Elementar Vario CNS Elemental Analyzer EL III. Reproducibility and accuracy were assured by running replicate analysis of laboratory reference materials and duplicate analysis of samples. The relative standard deviation was < 2%.

XRF

X-ray fluorescence measurements were carried out employing a Spectro XEPOS ED-XRF device. Here, 5 g of sample material was analyzed. To assure reproducibility and accuracy, a reference material was measured every 20 samples and the instrument was recalibrated, if the reference material (NCS DC 73326) was out of the certified limits. The relative standard deviation for the major elements (Si, Al, Ca, Fe, K, Na, P, Ti) was better < 1.5%. For trace elements (Mo, Zr, V, Cu, Mo, Cr) relative standard deviation was < 4% without U and including U < 6.5%.

Programmed pyrolysis

Programmed pyrolysis afforded a HAWK (Wildcat Technologies, US) instrument operated in pyrolysis and oxidation mode. An aliquot of 70 mg of sediment was weighted into a crucible and inserted by an autoloader into the HAWK device. Determination of thermo-vaporized bitumen (S1 in mg HC/g rock) occurred isothermally at 300 °C. The amount of kerogen was determined via the hydrocarbon yield upon pyrolysis (S2 in mg HC/g rock) through heating in an inert environment using a ramp rate of 25 °C from 300 to 650 °C. The pyrolysis measurements of both CO and CO_2 (S3CO in mg CO_2/g rock and $S3CO_2$ in mg CO_2/g rock) gave the oxygen concentration of the kerogen. The temperature of maximum pyrolysis yields recorded by the S2 peak is given as T_{max} (°C). The TOC was determined as the sum of reactive carbon (sum of bitumen and kerogen), analyzed in programmed pyrolysis mode in an inert environment, and the amount of non-generative carbon that was detected in oxygenated combustion mode. The carbonate content was determined via the release of CO_2 upon heating from 500 to 850 °C in oxidation mode and converted to calcite carbonate equivalents using a stoichiometry factor of 8.33.

Organic carbon isotope geochemistry

Organic carbon isotope analysis was performed on sample material decalcified by treatment with 10% and 25% HCl. Afterward, the decalcified sample residue was washed with deionized water until a pH of about 6. Measurements were carried out using a Thermo Finnigan Delta V isotope ratio mass spectrometer coupled to a Flash EA via a ConFlow III interface. The isotope ratio is expressed in the delta notation: $\delta sample(‰) = \left(\frac{RSample - RStandard}{RStandard} - 1\right) * 1000$ with R being the ratio of $^{13}C/^{12}C$ with V-PDB as reference material. Reproducibility and accuracy were assured by running replicate analysis of laboratory reference materials and duplicate analysis of samples.

Results

Results are described in stratigraphic order for the Intervals I–VI, which were defined by lithological criteria and geochemical data (I: Pliensbachian Amaltheenton Formation; II: basal Posidonia Shale Formation—pre T-CIE; III: Posidonia Shale Formation—T-CIE; IV: Posidonia Shale Formation—post T-CIE; V: Posidonia Shale Formation—Lower Elegans Bed; VI: upper Posidonia Shale Formation).

Bulk sediment composition

Relative abundances of the elements Si, Ti, Zr, and Al vary in dependency of the mineral content of sedimentary rocks,

such as the abundance of Al-rich clay minerals, Si-rich quartz and Zr-, Ti-rich heavy minerals (Taylor and McLennan 1985; Nesbitt and Young 1982; Brumsack 1991). Accordingly, Si/Al, Ti/Al, and Zr/Al ratios (supplement Table S1) can provide information on the composition of the clastic sediment fraction, in terms of mineral composition and grain size (sand, silt, clay). All ratios show a parallel evolution and correlation (supplement Fig. S1, Fig. S2). Accordingly, only the Zr/Al ratios is described here. The Zr/Al (ppm/%) ratios range from 22.9 to 8.5 (Fig. 3). In interval I, the ratio declines, reaching a minimum of 8.5 followed by a rapid increase in the uppermost part. This trend continues in the lowermost part of interval II and reaches values of about 16. An abrupt increase in Zr/Al ratios to values of about 22 occurs in the lowermost part of interval III. High but variable values of 16–23 are seen in lower and middle part of interval III, before a decrease to values of about 14 occurs in the upper part of interval III (Fig. 3). Interval IV shows an abrupt increase in the Zr/Al ratio to values around 17, followed by a plateau with steady values and a return to lower ratios of about 12 (Fig. 3). Mainly low Zr/Al ratios in the range 9–11 appear in interval V, while remaining higher of 16–18 in samples from interval VI (Fig. 3).

The chemical index of alteration (CIA) allows quantifying the chemical weathering intensity, whereby weathering and mineral hydrolysis will form Al-rich clay minerals, such as smectite and kaolinite (Nesbitt and Young 1982). The CIA adapted for carbonate-rich lithologies is calculated as $CIA^* = 100 * Al/(K + Na + Al)$. In the samples analyzed, the CIA* falls in the range of 66–80 (Fig. 3). The CIA* shows mainly high and steady values of 76–80 in samples from interval I, then decreases throughout the upmost part of intervals I and II. Mainly low but variable values of 66–76 occur in interval III (Fig. 3). An increase in the CIA* to about 75 occurs in the uppermost part of interval III. Increased by variable values in the range 70–80 were determined for intervals IV–VI, with more variable values in interval V (Fig. 3).

The carbonate contents range between 1 and 86% (Fig. 3, supplement Table S1). Carbonate contents are low in samples from interval I (1–3%) and successively increase in interval II to 24%. A sharp drop occurs in a heterolithic sample at the top of interval II (9%). Interval III is characterized by carbonate contents ranging from 9 to 41%. Toward the top of interval III, the values decrease and subsequently increase during interval IV before reaching a maximum of 86% in interval V. Samples from interval VI show carbonate contents in the range of 20–30% (Fig. 3).

Pyrite minerals can be considered the major host of the elements Fe and S (Berner and Raiswell 1983). The content

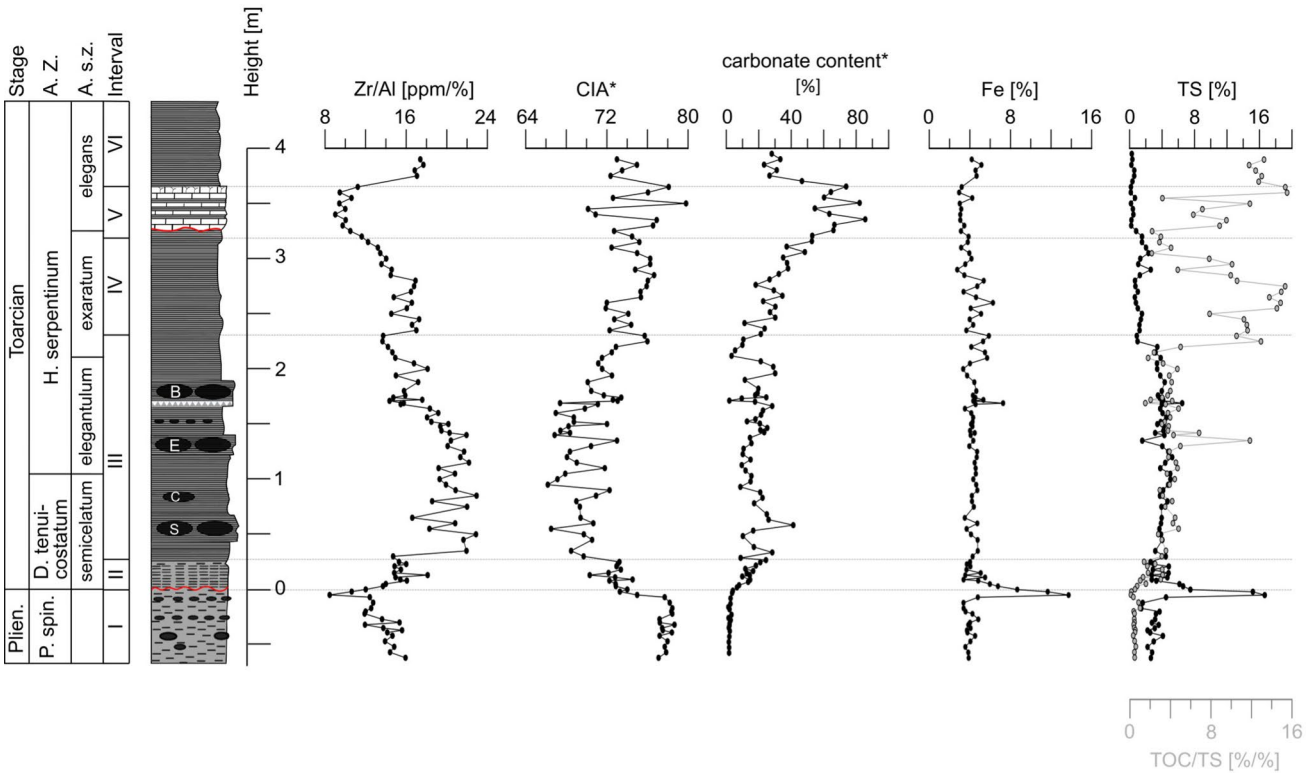

Fig. 3 Stratigraphic trends in Zr/Al ratios, the CIA*(modified Chemical Index of Alteration), carbonate content, as well as in the Fe and TS contents. For the lithological key, abbreviations and definition of the intervals, see Fig. 2

of Fe ranges from 3 to 13.7% (Fig. 3). Samples from interval I exhibit values mainly between 3 and 4%. The top of this interval is characterized by a horizon in which Fe abundances increase to values of 13.7%. In interval II, Fe abundances decrease to values in the range of 4–5%. Interval III is marked by mainly steady values in the range of 3–5%, with the exception of one sample with 7% and an increase to 4–5% in the uppermost part of the interval. In interval IV, the values remain in a similar range and drop toward the top to values of about 3%. Comparable values can be seen in interval V and increase to about 4–5% in interval VI (Fig. 3).

The TS contents fall in the range of 0.2–16.7% (Fig. 3, supplement Table S1). Throughout the intervals I–III, TS values mirror the trend seen in the Fe content. A drop in the TS content to values of about 1% is seen in the upper part of interval III. Lowered TS contents (mainly < 1%) are seen in samples from the intervals IV–VI (Fig. 3).

Bulk organic geochemical proxies

The $\delta^{13}C_{org}$ values range from − 26 to − 33.5‰ (Fig. 4, supplement Table S1). In intervals I and II, $\delta^{13}C_{org}$ steadily declines from − 26 to − 29‰. An abrupt change in the $\delta^{13}C_{org}$ from − 30 to − 33.5‰ is seen at the base of interval III that shows the overall lowest $\delta^{13}C_{org}$ values. An increase in $\delta^{13}C_{org}$ to values of about − 27‰ occurs in interval IV (Fig. 4). In intervals V and VI, $\delta^{13}C_{org}$ values range from − 28 to − 26‰.

The TOC content varies from 1.2 to 22.2% (Fig. 4, supplement Table S1). Mainly low TOC abundances in the range of 1–7% are seen in intervals I, V, and VI. Increased TOC abundances of 3.3–9.7%, 6.9–22.2%, and 7–15.7% occur in intervals II, III, and IV, respectively (Fig. 4). The S2 values vary between 1 and 157 [mg HC/g sediment] (Fig. 4). The S2 trend mirrors the observed TOC trend with mainly low values in the range of 1–5 [mg HC/ g sediment] in the intervals I, V, and VI and increased S2 values of 12–95 [mg HC/ g sediment], 32–157 [mg HC/ g sediment], and 23–88 [mg HC/ g sediment] in intervals II, III, and IV, respectively (Fig. 4).The HI ranges from 97 to 790 [mg HC/g TOC] (Fig. 4), with low HI values of 100–240 [mg HC/g TOC], 188–430 [mg HC/g TOC], and 186–400 [mg HC/g TOC] in intervals I, V, and VI, respectively. By contrast, high HI values of 337–790 [mg HC/g TOC] occur in intervals II–IV (Fig. 4). The OI values range from 7 to 129 [mg CO_2/g TOC] (Fig. 4). In interval I, OI values are 20–41 [mg CO_2/g TOC] and decline throughout this interval. Lowest OI values of 7–20 [mg CO_2/g TOC] occur in samples

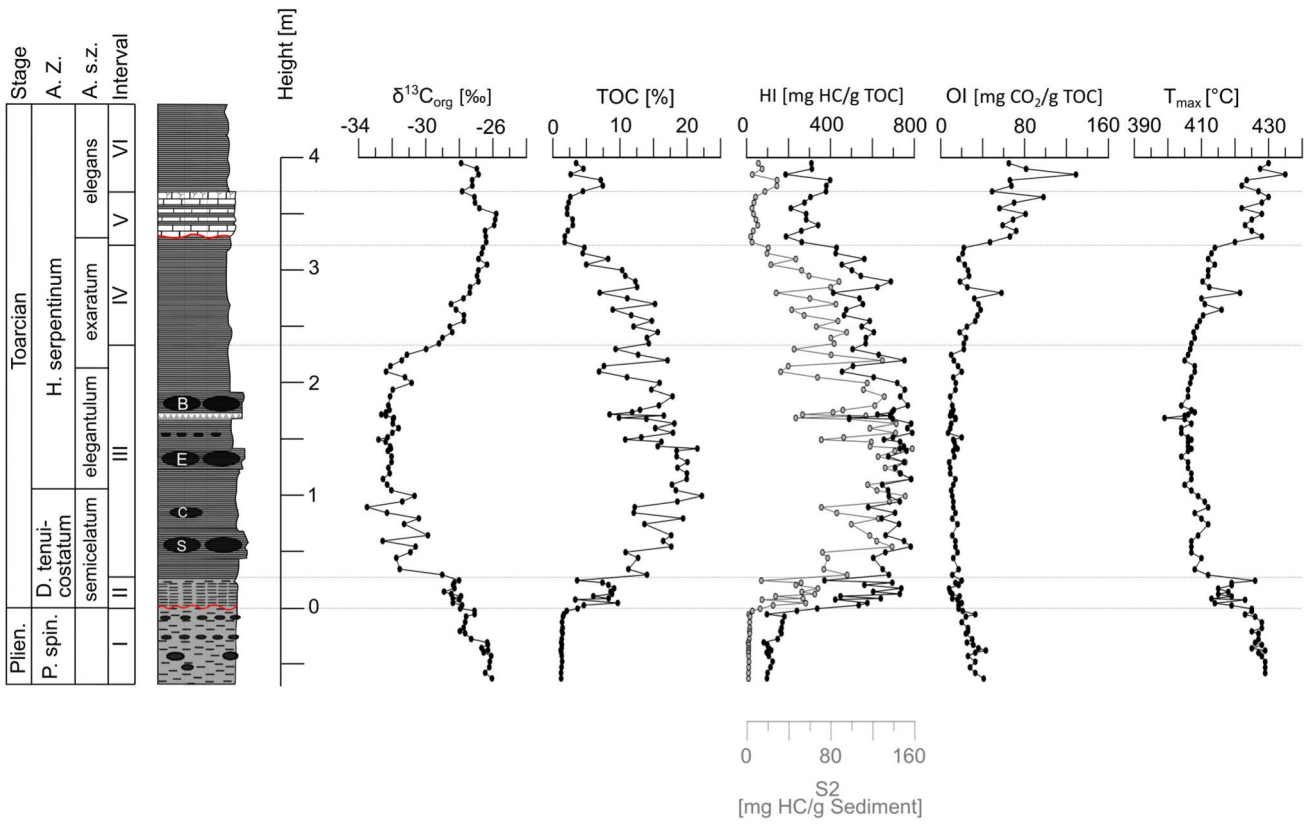

Fig. 4 Stratigraphic trends in $\delta^{13}C_{org}$, TOC, HI, S2, OI, and T_{max} values. For the lithological key, abbreviations, and definition of the intervals, see Fig. 2

from intervals II and III. Slightly increased OI values in the range of 17–58 [mg CO_2/g TOC] were observed in interval IV. The highest OI values of 21–129 [mg CO_2/g TOC] are seen in samples from intervals V and VI (Fig. 4). The T_{max} values vary between 399 and 435 °C (Fig. 4, supplement Table S1). Intervals I, V, and VI are characterized by high values of 413–435 °C. The intervals II, III, and IV show lowered values of 413–426 °C, 399–412 °C, and 407–416 °C, respectively.

Redox proxies

The content of selected redox-sensitive elements is expressed as abundance (ppm) and as enrichment factor (EF), relative to average shale values (Wedepohl, 1971, 1991). Enrichment factors were calculated as $X_{EF} = (X_{sample}/Al_{sample})/(X_{average\ shale}/Al_{average\ shale})$, with X representing the abundance of a redox-sensitive element (ppm) in the sample and average shale, respectively.

The abundances of Mo are 1.1–28.7 ppm, the Mo_{EF} values are 0.7–43 (Fig. 5). Interval I is characterized by low values of 0.7–1.2 increasing to 1–4 in interval II. At the base of interval III, enrichment factors strongly increase to 9.8–16.3. Lowered Mo_{EF} are observed in the upper part of interval III and lower part of interval IV (Fig. 5). Increased Mo_{EF} of about 30 are seen in the middle part of interval IV, before declining in the upper part. Within the lower part of interval V, low values range around 7.4–9.8. Subsequently the values increase reaching a maximum of 43 in interval VI.

Uranium abundance varies from 0 to 29 ppm. U_{EF} values range from 0 to 20.7 (Fig. 5, supplement Table S1). In interval I, low abundances of 0.1–1.1 were observed, thereafter increasing to 0.6–8.4 and 0.67–20.7 for intervals II and III, respectively. Shortly below the top of interval III, the values drop and remain low for intervals IV and V ranging from 0 to 7.8. In interval VI the values increase to 4.1–6.8.

The Cu abundances range from 17.7 to 116 ppm. The Cu_{EF} values are within the range of 0.4–5.1 (Fig. 5). Interval I shows low values between 0.4 and 0.7, thereafter increasing to values from 0.9 to 1.9 in interval II. In intervals III and IV, high values in the range of 1.8–4.1 were observed. The values decrease in interval V and range between 1.1 and 2.4. Interval VI is characterized by elevated values from 3.7 to 5.1.

The abundances of V vary from 91.6 to 389.4 ppm. V_{EF} values range between 1.1 and 3.9 for the succession. The trend closely resembles that of Cu_{EF} with elevated values in the range of 1.5–2, 1.7–3.4, 1.9–2.9, 1.7–3.1, and 3.3–3.9 for intervals II, III, IV, V, and VI, respectively, and low values ranging from 1.1 to 1.7 in interval I.

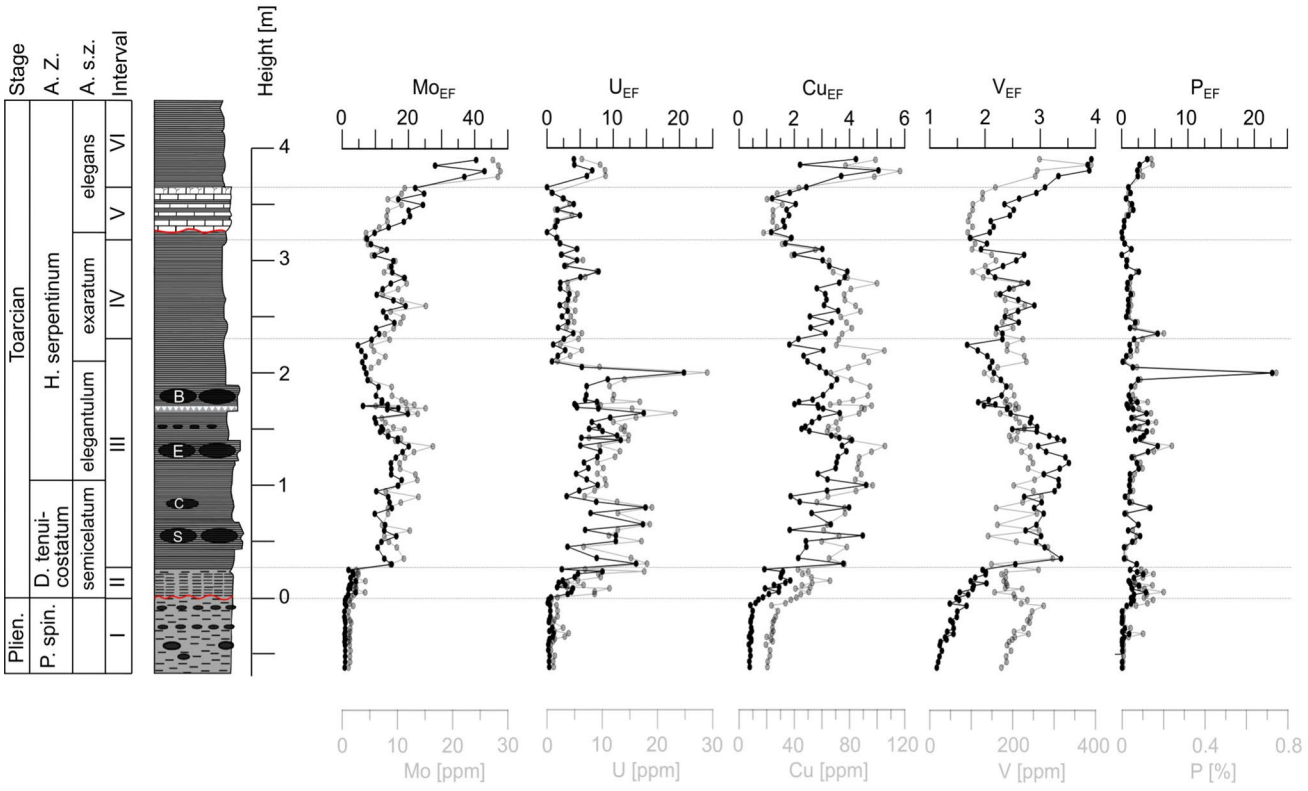

Fig. 5 Stratigraphic trends in abundances and enrichment factors (EF) of redox-sensitive elements. For the lithological key, abbreviations, and definition of the intervals see Fig. 2

P abundance varies from 0.0018 to 0.74%. P_{EF} values range between 0 and 22.7. Interval I is characterized by low values on the order of 0.1–1.8. Subsequently, the values remain elevated for intervals II, III, and IV although with large fluctuations ranging from 0.1 to 22.7. At the beginning of interval V, the values are decreased at 0–1.5 but subsequently increase and exhibit high values ranging from 2.4 to 3.9 for interval VI. The highest value of 22.7 is attributed to fish debris (Delaney 1998).

Discussion

Sample quality

Surface samples, collected in an outcrop, such as those studied here, can be affected by weathering, resulting in alteration of mineral assemblages (Littke et al. 1991a, b), element contents (Marynowski et al. 2017) and organic matter composition (Bordenave et al. 1993). Pyrite/sulfides and organic matter are most sensitive toward weathering (Littke et al. 1991a, b; Marynowski et al. 2017; Ruebsam et al. 2018). Accordingly, weathering-related alteration of the sample material can be inferred from characteristic TOC/TS ratios (Ruebsam et al. 2018).

Suspiciously high TOC/TS ratios of 4–18 occur in samples from intervals VI, V, and IV, suggesting oxidation of pyrite/sulfides via meteoric waters. Comparable TOC/TS ratios of 4–24 were determined for the Toarcian Hainberg outcrop section located app. 70kms SSW of Hondelage by Arp et al. (2023). In contrast, the TOC/TS ratios determined for the nearby Schandelah core by Ruvalcaba Baroni et al. (2018) yielded TOC/TS ratios for the T-OAE of around 2.2, indicative of pristine pyrite. A compilation (Brumsack 1991) of TOC/S ratios for the NGB gave an average value of 2.3. Core data lacking effects of weathering, thus, yield TOC/S ratios in the region proposed for the average anoxic marine shale value of 2.5 (Berner and Raiswell 1983). The close proximity between the Hondelage and Schandelah sites precludes drastic changes in environmental conditions, e.g., sulfate depletion by brackish waters, affecting the TOC/TS ratios and, thus, support the interpretation that both the Hondelage and Hainberg outcrop section are affected by pyrite weathering. This is compatible to the T-OAE section in Reka Valley (Ruebsam et al. 2018), where TOC/S ratios in the weathered part of the section increased to on average values of 26, whereby the hydrophobic organic matter showed almost no effect of oxidation (see supplement Fig. S3).

Uranium dissolves easily when exposed to oxidative fluids (Perkins and Mason 2015), which may explain the abrupt decline in U concentrations and U_{EF} in the upper part of interval III (Fig. 5). This indicates that U has potentially been altered over parts of intervals IV–VI and data must be interpreted with caution. The redox-sensitive elements Mo, Cu, V, and P show no evidence for strong weathering-related alterations. Abundances and enrichment factors are lowered in the Lower Elegans Bed (interval V) but increase in interval IV to values comparable to those seen in interval III, which appears to be unaffected by surface weathering. Mo even reaches its strongest enrichment in interval VI (Fig. 5). Sedimentary organic matter can also be affected by outcrop weathering leading to a decline of HI and TOC, as well as to an increase in OI (Bordenave et al. 1993; Ruebsam et al. 2018). Lowered TOC and HI values accompanied by increased OI values occur in intervals V and VI. Samples from both intervals show increased T_{max} values (Fig. 4). This pattern may point to syndepositional changes in organic matter preservation, superimposed by weathering-related changes in organo-facies. In particular, high OI values accompanied by high/moderate TOC and moderate HI values point to oxidation of sedimentary organic matter via surface weathering. Consequently, data from the intervals V and VI are most likely altered by outcrop weathering, and U, TS, and organic proxies should be interpreted with caution.

Stratigraphic evaluation and correlation

Precise stratigraphic correlation can be based on the combination of bio- and chemostratigraphic approaches (see review by Gröcke (2020) and references therein). For the late Pliensbachian and the early Toarcian, characteristic trends in organic carbon isotopes, such as the P/T-CIE and the T-CIE, have proven their chemostratigraphic correlation potential (e.g., Hesselbo et al. 2000, 2007; Ruebsam and Al-Husseini 2020). Combined application of bio- and chemostratigraphic approaches further allows to assess the stratigraphic completeness of a sediment archive and to detect potential hiatuses as well as condensed intervals (Pittet et al. 2014; Gröcke 2020; Ruebsam and Al-Husseini 2020).

For the Hondelage succession, the presence of stratigraphic gaps is indicated by biostratigraphic and lithological data (Mutterlose et al. 2022), which suggests a substantial gap at the Pliensbachian/Toarcian boundary (boundary interval I/II), covering the lower part of the *D. tenuicostatum* Zone. A belemnite battle field, consisting of corroded rostra, marks the boundary. Comparable lack of the basal Toarcian strata has been reported for the Wickensen and Mainzholzen sites of the Hils Syncline (Burnaz et al. 2024). The Lower Elegans Bed (*H. serpentinum* Zone; interval V) exhibits an erosive base, the potential hiatus is in this case minor.

The stratigraphic completeness of the Hondelage succession can further be assessed by chemostratigraphic correlation with coeval sediment archives for which detailed bio- and chemostratigraphic data are available. We here discuss the chemostratigraphy of the Hondelage section and its correlation with the nearby Schandelah Core (N-German

Basin; Ruvalcaba Baroni et al. 2018, van de Schootbrugge et al. 2019; Visentin et al. 2022; Ruebsam et al. 2024), the Rietheim core (SW-German Basin; Montero-Serrano et al. 2015) and core FR-210-078 (Lorraine Sub-Basin, Paris Basin, Luxembourg; Ruebsam et al. 2019). The Schandelah core is located about 8 km to the southeast of the Hondelage section. Accordingly, ammonite zones and $\delta^{13}C_{org}$ trends are comparable to those seen in Hondelage. At both sites, the *D. tenuicostatum* Zone is extremely condensed and only represented by the *D. semicelatum* subzone (Fig. 6). The abrupt decline in $\delta^{13}C_{org}$ values, marking the onset of the negative T-CIE, directly starts in the interval above the Pliensbachian/Toarcian boundary. This pattern of carbon isotope trends indicates that most of the lower *D. tenuicostatum* Zone and most likely the Pliensbachian/Toarcian boundary interval is missing in Hondelage and Schandelah. A comparable pattern is seen in the Rietheim Core from the South-German Basin, where the Pliensbachian/Toarcian boundary is directly followed by the negative T-CIE, whereby the *D. tenuicostatum* Zone is condensed. Moreover, in the Rietheim succession, the Pliensbachian/Toarcian boundary is marked by an erosive horizon (Montero-Serrano et al. 2015). At these three sites, the *D. tenuicostatum* Zone is condensed and lithological data attest to the presence of a major hiatus. Moreover, a P/T-CIE is not clearly expressed in the $\delta^{13}C_{org}$ data. Accordingly, the Pliensbachian/Toarcian boundary interval is most likely not preserved at Hondelage, Schandelah and Rietheim (Fig. 6).

In contrast, the *D. tenuicostatum* zone is more expanded in core FR-210.078 (Luxembourg) and the Pliensbachian/Toarcian boundary is indicated by the P/T-CIE (Ruebsam et al. 2019). This suggests that basin morphology in combination with sea-level fluctuations controls the deposition and stratigraphic completeness as indicated by previous works (Pittet et al. 2014; Ruebsam et al. 2019, 2020b, 2024; Ruebsam and Al-Husseini 2020; Ruebsam and Schwark 2024). Stratigraphic gaps are most pronounced at the Pliensbachian/Toarcian boundary interval and in the *D. tenuicostatum* Zone. This interval corresponds to marked sea-level lowstands, which at shallow sites led to erosion and the development of hiatuses (Hallam 1997; Morard et al. 2003; Wignall 2005; Pittet et al. 2014; Krencker et al. 2019; Ruebsam et al. 2020b, 2024; Bodin et al. 2023). The preservation of the P/T-CIE in Luxemburg suggests that this basin was deeper and, hence, not affected by erosion during sea-level lowstand in the early *D. tenuicostatum* Zone (Ruebsam et al. 2019). Accordingly, the sites Hondelage, Schandelah, and Rietheim may represent more shallow depositional settings that were prone to erosion or winnowing by contour currents upon sea-level lowstands. The onset of the negative T-CIE is very abrupt in Rietheim and in Luxemburg, which points to sediment starvation and stratigraphic condensation upon the early Toarcian transgression (Ruebsam et al. 2019). On the contrary, a more gradual decline in the $\delta^{13}C_{org}$ values is seen at Hondelage and Schandelah (Fig. 6).

Data from the Hondelage succession and comparison with coeval strata from adjacent basins highlight the role of sea-level fluctuations and basin morphology as a major factor controlling the stratigraphic completeness of Early Toarcian sediment archives. Data indicate a major sea-level lowstand immediately prior to the T-CIE, while the T-CIE coincides with a major transgression and a sea-level highstand. Moreover, at Hondelage, a sea-level fall is indicated for the post T-CIE interval by an erosive horizon at the base of the Lower Elegans Bed (Fig. 2c). Evidence for erosive events at coeval stratigraphic intervals were documented for the Paris Basin (Hermoso et al. 2013; Thibault et al. 2018), or the Lusitanian Basin (Pittet et al. 2014). Data thereby attest to dynamic sea-level changes, not only prior to the T-CIE, but also after the T-CIE (Ruebsam et al. 2020b; Schwark and Ruebsam 2024).

Sediment composition and evolution of the depositional setting

The sediment composition of marine basins is controlled by the interplay of sea-level fluctuations, climate, primary productivity, depositional conditions, weathering in the catchment area, runoff, and the position of river mouths. The general composition of marine sediments can be described as four-component system, composed of siliciclastics [= 100%—carbonate (%)—organic matter (%)—pyrite (%)], carbonates, organic matter (= TOC × 1.3) and pyrite (= TS × 1.7) (e.g., Ricken 1993; Röhl et al. 2001; Burnaz et al. 2024). A major change in the sediment composition occurred throughout interval II that records an increase in the relative abundance of carbonate and organic matter (Fig. 7). A minor increase in pyrite is seen as well, whereby the interval I/II boundary records a marked pyrite spike.

Overall low carbonate abundances in interval I (Pliensbachian) are explained by a low-productive, shallow marine environment, in which marine biocalcifiers, such as calcareous nannoplankton, were scarce (Mutterlose et al. 2022; Visentin et al. 2022). Therefore, the Pliensbachian Amaltheenton strata is strongly dominated by clastic sedimentation. In intervals II–VI, increased carbonate abundances can be linked to enhanced contributions from calcareous nannoplankton, a major source of the sedimentary carbonate fraction (e.g., Mattioli et al. 2008; Mutterlose et al. 2022; Visentin et al. 2022). During deposition of intervals II–VI, a higher sea level favored higher abundances of calcareous nannoplankton, even though these organisms experienced a marked crisis during the T-OAE or "Jenkyns Event" (e.g., Mattioli et al. 2008; Ruebsam et al. 2022c). This biocalcification crisis might be expressed by moderate carbonate abundances

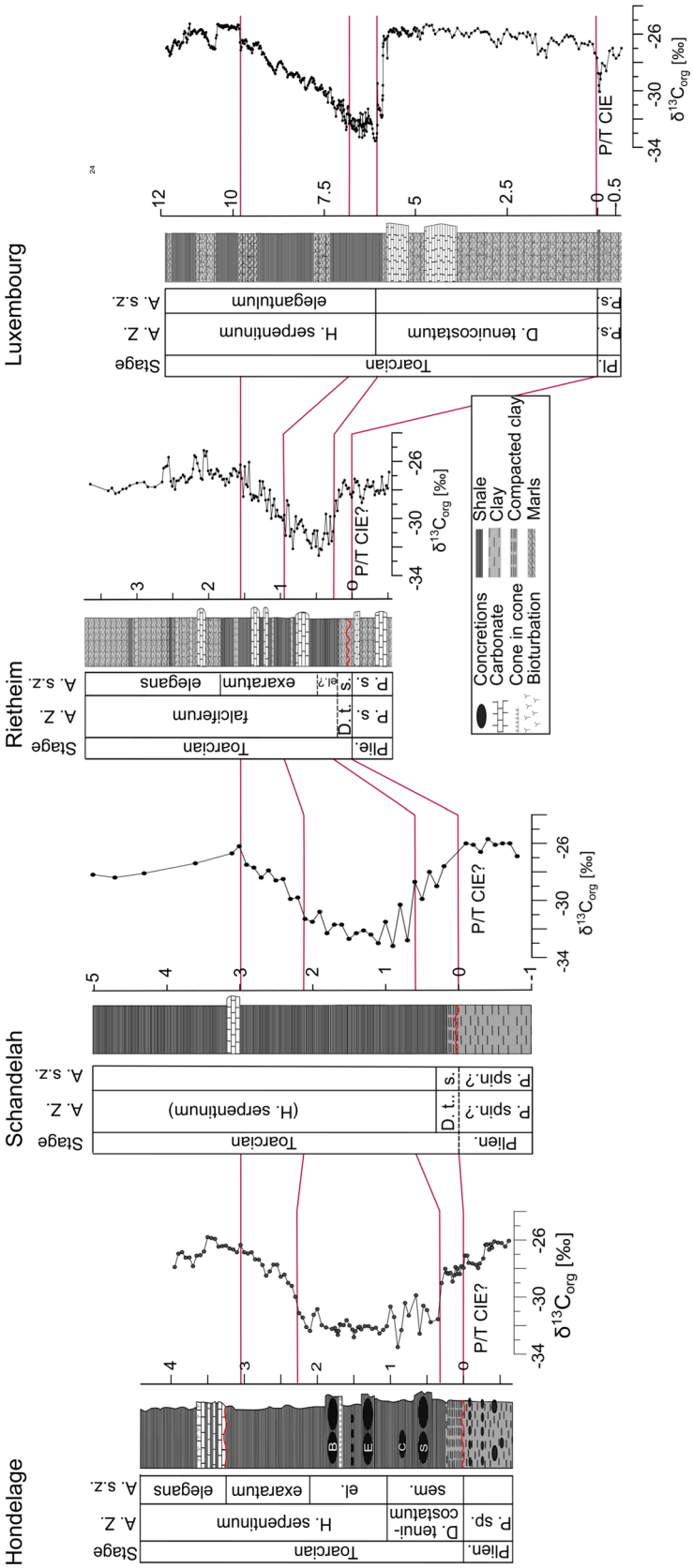

Fig. 6 Bio- and chemostratigraphic correlation of Late Pliensbachian–Early Toarcian sediment archives from the NGB, South-German Basin (SGB), and Paris Basin. NGB, Hondelage: This study and Mutterlose et al. (2022). NGB, Schandelah: Ruvalcaba Baroni et al. (2018); Van de Schootbrugge et al. (2019), Visentin et al. (2022). SGB, Rietheim; Montero-Serrano et al. (2015). Paris Basin, Lorraine Sub-Basin, Luxembourg: Ruebsam et al. (2019). Due to the lack of age diagnostic macrofossils, the ammonite biostratigraphy for Schandelah above the *D. tenuicostatum* Zone remains uncertain (see van de Schootbrugge et al. (2019) and Fig. 2)

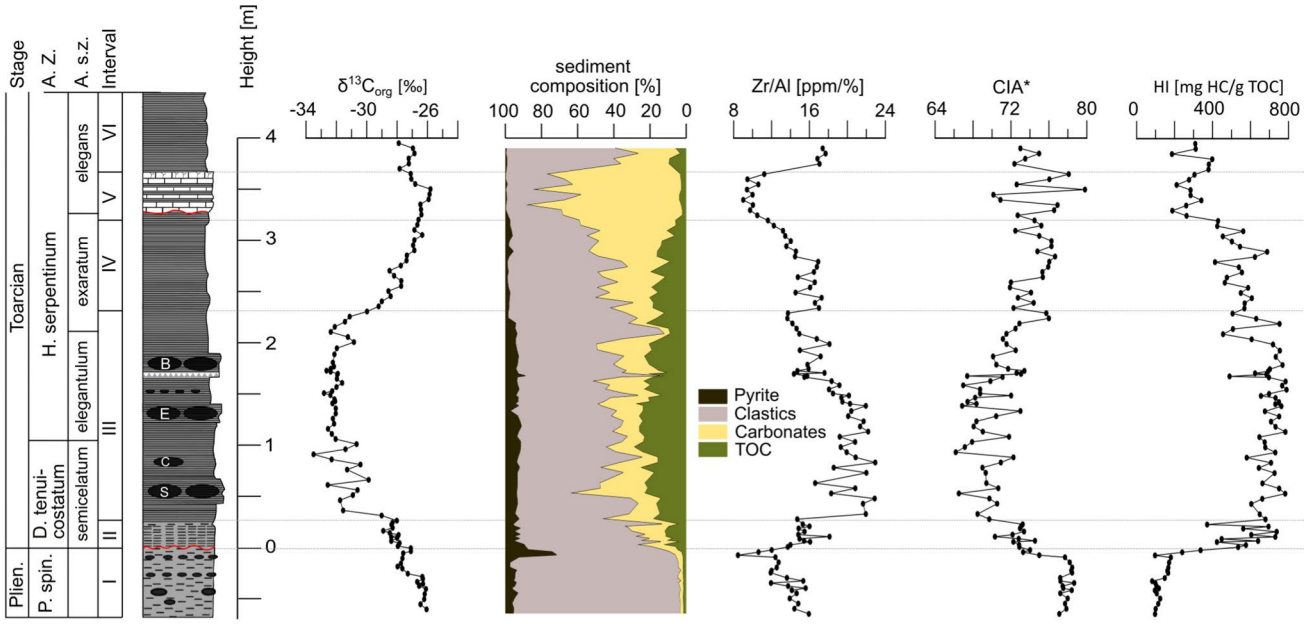

Fig. 7 Stratigraphic trends in $\delta^{13}C_{org}$, four-component gross sediment composition for pyrite, clastics, carbonates, and TOC, Zr/Al ratios, CIA* (modified Chemical Index of Alteration), hydrogen index (HI) from programmed pyrolysis

in interval III (Fig. 7). Carbonate abundances increase in interval IV and maximize in interval V (Lower Elegans Bed), indicative of a recovery of calcareous nannoplankton subsequent to the Jenynks Event (Mattioli et al. 2008, 2009; Hermoso et al. 2009; Ruebsam et al. 2022c). Marked fluctuations occur in carbonate contents of interval III. Caution must be taken here as syn-/post-depositional growth of carbonate concretions, abundant in this interval, was most likely associated with the redistribution of bulk sedimentary carbonate.

In interval I, low organic matter (and TOC) abundances accompanied by low HI and moderate OI values attest to a well-oxygenated shallow marine depositional setting unfavorable for the preservation of labile marine organic matter. Increased organic matter abundances, high HI and low OI values occur in intervals II–IV, which indicates the presence of well-preserved labile marine organic matter deposited in a low-energetic setting, below the wave/storm base, under preferentially oxygen-deficient conditions (Fig. 7). Changes in redox regime, but in the Hondelage outcrop also weathering controlled trends in pyrite abundances. The pyrite spike at the interval I/II boundary may reflect post-depositional diagenetic pyrite formation in strata underlying the Posidonia Shale Formation. Lowered organic matter abundances in interval V are best explained by carbonate dilution (Fig. 7). In intervals V and VI, lowered organic matter and pyrite abundances may be affected by outcrop weathering.

Interplay of sea level, continental weathering, and fluvial discharge

Changes in the composition of the siliciclastic sediment fraction, in terms of its grain-size (sand, silt, clay) and clay assemblages (e.g., kaolinite, smectite, illite, chlorite), will vary as function of sea level and associated shifts in the shoreline, as well as clastic influx via fluvial discharge and continental weathering (Nesbitt and Young 1982; Taylor and McLennan 1985; Ganeshram et al. 1999; Dypvik and Harris 2001; Dera et al. 2009; Govin et al. 2012; Hermoso et al. 2013).

In intervals II–IV, an increase in the Zr/Al ratio (and Si/Al, Ti/Al), accompanied by a decline in the CIA* (Figs. 7, 8a, and Fig. S3), reflects an increase in grain size of the clastic fraction and the presence of less-hydrolyzed clay mineral assemblages (Nesbitt and Young 1982; Taylor and McLennan 1985). The coarser grain size is explained by higher transport energy via enhanced riverine runoff during an intensified Toarcian hydrological cycle (e.g., Cohen et al. 2004; Brazier et al. 2015; Izumi et al. 2018; Krencker et al. 2020). At Hondelage, grain-size variation of the clastic sediment fraction was primarily driven by changes in riverine runoff, counterbalancing a fining upward trend associated with the early Toarcian transgression (Ruebsam et al. 2019). The complex interplay of continental runoff and sea-level change is expressed by the heterogeneity of grain-size proxies seen in coeval strata elsewhere (e.g., Dera et al. 2009;

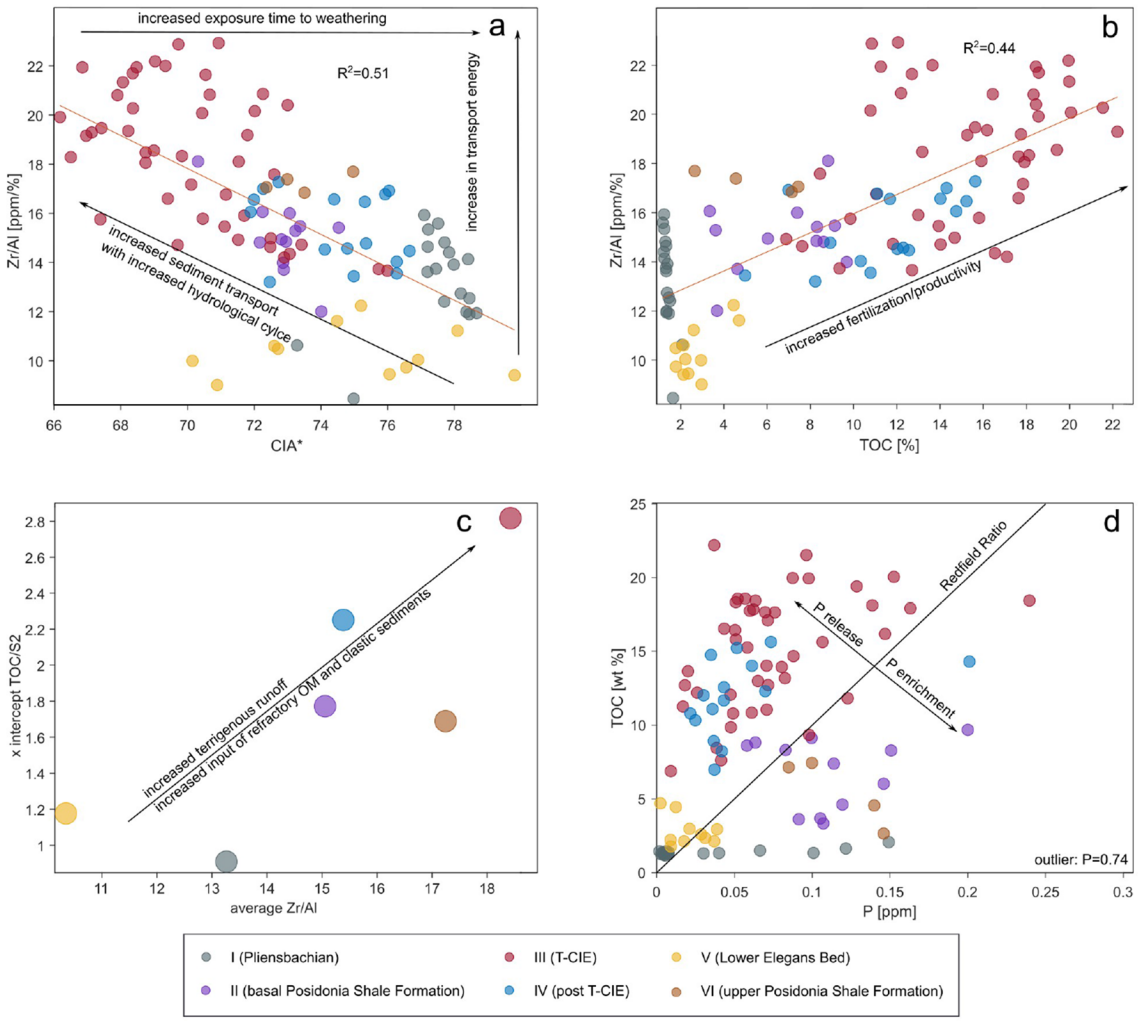

Fig. 8 **a** Positive correlation of Zr/Al ratio *vs.* CIA* indicates increased transport efficiency of clastic material via an enhanced hydrological cycle. **b** Zr/Al ratio *vs.* TOC shows a positive correlation suggesting nutrient delivery via terrestrial runoff. **c** x-axis intercept of TOC/S2 regression line *vs.* Zr/Al ratios averaged for the respective intervals (I–VI) indicating increased erosion of refractory organic matter from terrestrial sources (presumably soils) via an increased hydrological cycle. **d** TOC *vs.* P indicating P release from the sediment under reducing conditions for values above the Redfield ratio (Redfield 1958). Samples plotting below the line indicate P enrichment either by precipitation of authigenic apatite (Jarvis et al. 1994; Reimers et al. 1996) or fish debris (Delaney 1998)

Hermoso et al. 2013; Montero-Serrano et al. 2015; Xu et al. 2018; Fantasia et al. 2019; Ruebsam et al. 2019).

The decline of the CIA* seems to contradict the widely accepted model of an accelerated hydrological cycle and increased chemical weathering during the T-CIE (e.g., Cohen et al. 2004; Dera et al. 2009; Hermoso et al. 2013; Brazier et al. 2015; Xu et al. 2018; Kemp et al. 2020). Data from coeval strata show an increase in the relative abundance of chemically altered clay mineral assemblages dominated by smectite and illite (Dera et al. 2009; Montero-Serrano et al. 2015; Xu et al. 2018; Burnaz et al. 2024).

At Hondelage, the relative increase in abundance of less-hydrolyzed clay minerals and coarse-clastics might point to a proximal source area from which coastal-plain bedrock sediment was rapidly eroded and transported to adjacent marine areas. Either, erosion of freshly exposed bedrock occurred rapidly prohibiting intensive hydrolysis of the transported material (Figs. 7, 8a) and/or costal-plain sediments contained weathering residues rich in quartz and heavy minerals. Such a scenario is in agreement with an intensified hydrological cycle and substantial strengthening of riverine discharge to the EEBS (e.g., Cohen et al. 2004; Montero-Serrano et al. 2015; Xu et al. 2018; Kemp et al. 2020), although changes in catchment area and, hence, source region cannot be excluded. This scenario is further supported by the palaeogeographic setting of the study site located in the Oberaller Through in close proximity to exposed land masses, such as the Bohemian Massif to the

east, the Calvörde and Altmark Swells/Islands to the north and the Fallstein Swell/Island to the south (Fig. 2b). Thus, short transport distances facilitated proximal marine deposition of both fine and coarse-grained terrigenous clastics.

The clastic input and grain size decline in the T-CIE recovery interval (interval IV) toward the Lower Elegans Bed (interval V), which may mark a weakening of the hydrological cycle and longer sediment exposure times to chemical weathering, might have caused a slightly increased CIA* (e.g., Cohen et al. 2004; Montero-Serrano et al. 2015; Kemp et al. 2020). This presumably was related to colder temperatures (Ruebsam et al. 2020a). In interval VI, an increase in Zr/Al ratios is not accompanied by changes in the CIA* and may reflect the increase in transport energy during a lowered sea level, changes in river mouth or delta system position (Figs. 7, 8a).

Organofacies and organic matter accumulation

Organofacies characterization

Organofacies characterization is based on programmed pyrolysis-derived proxies (HI, OI, T_{max}). Low to moderate T_{max} values (< 430 °C; 415 °C on average) attest to an overall low thermal maturity of the sedimentary organic matter. The variability of the T_{max} reflects differences in the stability of the kerogen toward thermal breakdown and, thus, differences in the kerogen composition. Low HI (< 200 mgHC/gTOC) and slightly increased OI (20–45 $mgCO_2$/gTOC) values in TOC-lean samples from interval I indicate the presence of mainly degraded marine organic matter, as well as minor contributions from land plants. Moreover, increased T_{max} values suggest the presence of recalcitrant kerogen in sediment of interval I, the destruction of which requires higher temperatures (Espitalie et al. 1985; Bordenave et al. 1993; Stock et al. 2017). In interval I, mainly low Zr/Al ratio argues for a low influx of clastic material from adjacent land masses, suggesting that organic matter contributions from land plant sources were low as well. Low HI values could indicate that relative contributions of terrigenous organic matter may have been elevated by even more diminished flux of marine organic matter. Enhanced terrigenous wax lipid fluxes during deposition of the Amaltheenton Fm. was proposed by Burnaz et al. (2024) based on a dominance of long-chain *n*-alkanes found in sediments of the Hils syncline.

Increased HI values (mainly > 500 mgHC/gTOC) and low OI values (< 20 $mgCO_2$/gTOC), as seen in the TOC-rich intervals II–IV, indicate the presence of high abundances of labile marine organic matter originating from algae and bacteria. The lowest T_{max} values were observed in intervals II–IV supporting this interpretation and indicating the presence of labile kerogen, whose thermal breakdown requires less energy (Espitalie et al. 1985; Stock et al. 2017). Moderate HI, accompanied by increased OI and T_{max} values, is seen in samples from intervals V and VI. In particular, high OI and T_{max} values point to the alteration of sedimentary organic matter by outcrop weathering. Thus, a reliable organo-facies assessment is hampered for these intervals.

Primary productivity

In marginal marine environments, such as in epicontinental seas, marine primary productivity will be maintained by the nutrient supply from adjacent land masses (van Helmond et al. 2015). In particular, areas in proximity to estuaries and deltas can considered being highly productive (Bianchi and Allison 2009). The evolution of clastic proxies (Zr/Al, CIA*) indicate that the setting of Hondelage, located in proximity to the north-western wedge of the Bohemian Massif and also close to some smaller islands (Fig. 2b), presumably was strongly affected by changes in the continental runoff, clastic influx and weathering intensity. Samples from the Pliensbachian (interval I) are characterized by low TOC abundances, Zr/Al ratios, and high CIA* values. In contrast, highest TOC abundances accompanied by increased Zr/Al ratios (and decreased CIA*) are seen in intervals II–IV (Fig. 8a, 8b), corresponding to the T-CIE (interval III). During the Jenkyns Event, intensified hydrological cycling led to enhanced mobilization of nutrients that were transported to marginal marine settings and maintained a high primary productivity. The positive relationship of TOC and Zr/Al ratios indicates that at this marginal marine setting, changes in continental runoff and nutrient supply directly impacted marine primary productivity and organic matter burial (Fig. 8b). This interpretation is supported by the pattern seen in Zr/Al ratios and the x-axis intersect of the TOC/S2 binary diagram (see supplement Figs. S4 and S5) averaged for the different intervals (Fig. 8c). Hereby, the TOC-axis intercept value indicates the proportion of refractive organic carbon derived from reworked terrigenous biomass (Fig. 8c, Fig. S4). Highest x-axis intercepts of the TOC/S2 regression line, along with increased average Zr/Al ratios, occur for intervals II–IV (Fig. 8c), and indicate that the refractory organic matter originated from terrigenous sources and became remobilized via surface weathering and erosion. The enhanced delivery of terrigenous soil organic matter and associated nutrients presumably fostered primary productivity at marginal marine areas.

Additionally, the establishment of reducing conditions might have caused phosphorous release from the sediments (Tyson and Pearson 1991; Ingall et al. 1993; van Cappellen and Ingall 1994). Phosphorous often is a limiting nutrient that is sequestered in the sediments under oxic conditions (Jarvis et al. 1994; Reimers et al. 1996). A release of

P becomes evident from TOC/P ratios. A strong deviation from the Redfield ratio (106:16:1, C:N:P (Redfield 1958)) toward higher values indicates the release of P from the sediments. The proposed elevated frequency of cyclones with the establishment of green/hothouse conditions during the onset of the T-CIE (Korty et al. 2008; Krencker et al. 2015) and also in the period thereafter (Schwark and Ruebsam 2024) might have induced upwelling of deep P- and nutrient-enriched waters further promoting surface water productivity (Fig. 8d).

Redox regime

The T-OAE caused the expansion of oxygen-deficient conditions in shelf seas, epicontinental seas and potentially in deep oceanic settings (e.g., Jenkyns 1988, 2010; Kemp et al. 2022). Redox conditions prevailing in pore and bottom-waters can be inferred from sedimentological characteristics (e.g., Wignall 1991), the enrichment pattern of redox-sensitive elements, such as U, Mo, Cu, or V (e.g., Algeo and Maynard 2004; Tribovillard et al. 2006), from TOC-TS-Fe systematics (Berner and Raiswell 1983) or from fossil assemblages (Röhl et al. 2001), including trace fossil associations (Savrda and Bottjer 1986) and coupled biomarker and fossil indicators (Frimmel et al. 2004).

The TOC-lean Pliensbachian (interval I) samples lack an enrichment of redox-sensitive element (Figs. 5, 9). Moreover, organic matter in samples from this interval was subjected to intense aerobic degradation, as indicated by low HI and increased OI values. Data attest to a well-oxygenated shallow marine depositional environment not favorable for the preservation of labile marine organic matter. This

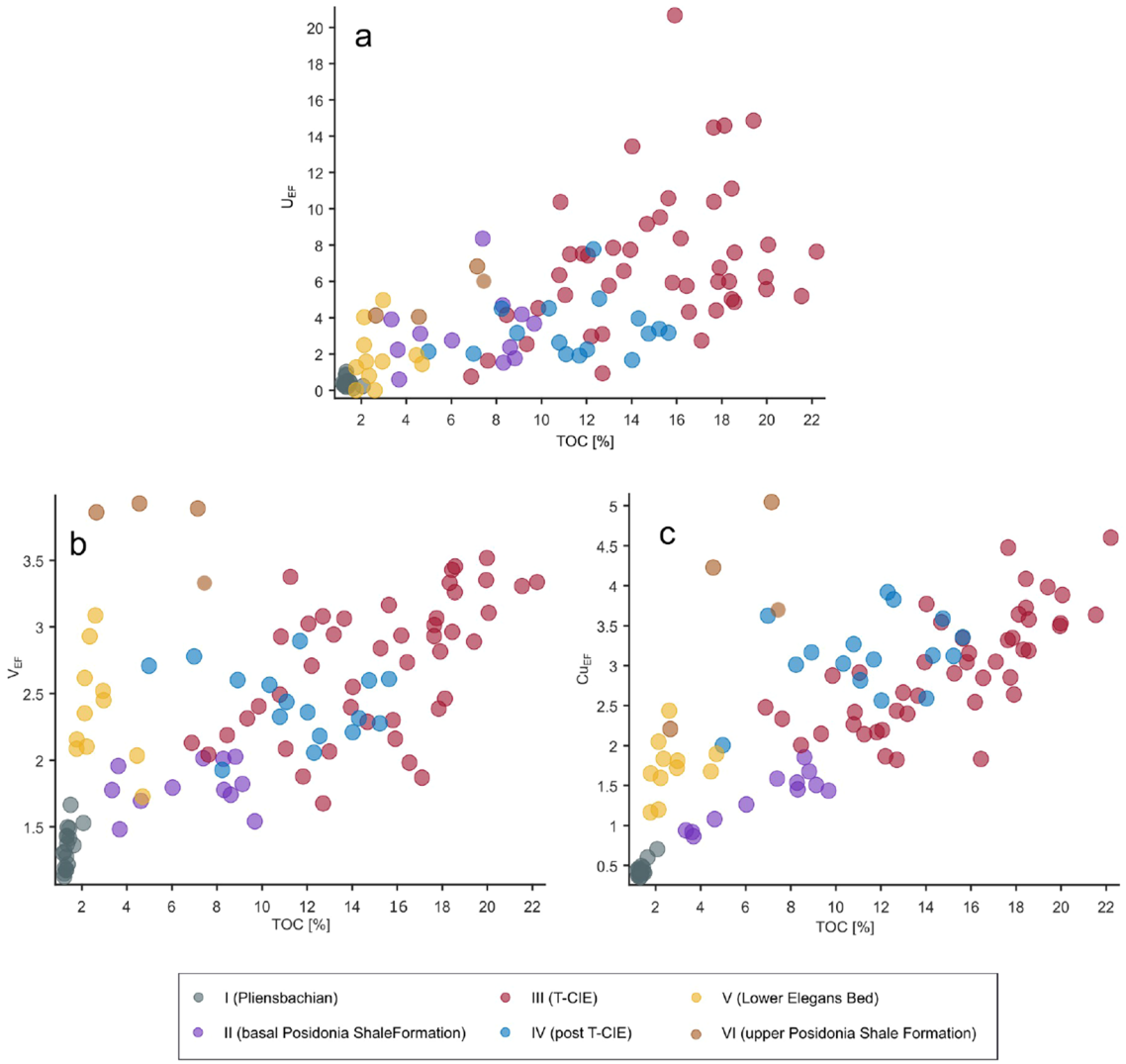

Fig. 9 Binary diagrams of redox-sensitive trace elements *vs.* TOC. **a** U_{EF} *vs.* TOC, intervals IV–VI are affected by the loss of U due to outcrop weathering. **b** V_{EF} *vs.* TOC, **c** Cu_{EF} *vs.* TOC

interpretation is consistent with data from coeval strata from the wider EEBS, which commonly lack evidence for reducing conditions (e.g., Hermoso et al. 2013; Montero-Serrano et al. 2015; Ruvalcaba Baroni et al. 2018). Under these conditions, the chemocline was predominantly localized within the sediment and no oxygen-deficient conditions could develop at the sediment–water interface or in the water column.

An initial increase in TOC and redox-sensitive elements is seen in the Toarcian interval II. In particular, an increase is seen in Cu_{EF} and U_{EF}, while V_{EF} and Mo_{EF} show a minor increase only (Figs. 5, 9). The increase in Cu_{EF} and U_{EF}, attest to an enhanced organic matter flux to the sediment and the expansion of suboxic-anoxic conditions. Low enrichment factors seen for the elements Mo and V indicate that anoxic–euxinic conditions may not have developed over longer periods of time (Algeo and Maynard 2004; Tribovillard et al. 2006). Toarcian interval II corresponds to the onset of the T-CIE and the early-stage T-OAE marked by an initial sea-level rise and an increase in marine primary productivity, as indicated by clastic proxies and calcareous nannofossil evidence (Mutterlose et al. 2022). Highest TOC abundances along with high HI values and a substantial enrichment of Cu and V are noted for samples from intervals III and IV. An enrichment of U is lacking in interval IV, but this may be affected by outcrop weathering. Data argue for a substantial increase in marine organic matter flux and establishment of prolonged anoxic–euxinic conditions in the intervals marking the T-OAE climax. During this time, high temperatures, intensified hydrological cycling and increased runoff provided substantial amounts of nutrients to marginal marine areas, thus maintaining a high primary productivity that subsequently favored the development of oxygen-deficient conditions in pore- and bottom-waters (Cohen et al. 2004; Brazier et al. 2015; Izumi et al. 2018). Moreover, increased runoff will have promoted freshwater stratification limiting the vertical ventilation of the water column (Riegel et al. 1986; Brumsack 1991; Saelen et al. 1996; Röhl et al. 2001; Schwark and Frimmel 2004), thus initiating oxygen-deficiency in pore- and bottom-waters. The sea-level highstand during the T-CIE initiated a basinwide expansion of low-energy depositional settings favoring the preservation and accumulation of TOC-rich strata (Wignall 1991; Röhl et al. 2001).

Enrichment factors for Cu and V, as well as TOC abundances decline in interval V (Lower Elegans Bed) (Figs. 5, 9). Here, evidence of sediment reworking, erosion, and bioturbation, which indicate sea-floor ventilation suggest a lowered sea level (Mutterlose et al. 2022). In the Sancerre Core (southern Paris Basin), sea-floor re-oxygenation events have been documented from a comparable stratigraphic position (Hermoso et al. 2013). A return to predominantly anoxic/euxinic conditions in the interval VI can be inferred from increasing TOC, Mo_{EF}, Cu_{EF}, and V_{EF} (Fig. 5, 9). This interval corresponds to a sea-level rise, which impacted on the depositional and redox conditions (Röhl et al. 2001; Frimmel et al. 2004; Hermoso et al. 2013; Ruebsam et al. 2019). Data from Hondelage thereby highlight the role of sea-level change as a major process modulating the redox environment during the late Pliensbachian to early Toarcian times.

Basinal restriction and hydrology

Molybdenum is a conservative element in the modern ocean with an average concentration of 105 nmol/kg and a residence time of 800 ka (Emerson and Huested 1991). Under anoxic/euxinic conditions, Mo is efficiently scavenged from the water column in the form of thiomolybdate complexes leading to an accumulation of Mo in the sediment (Helz et al. 1996). In restricted basins, where Mo scavenging exceeds the resupply, Mo can become depleted in seawater over time (Algeo and Maynard 2004; Algeo and Lyons 2006). Under such conditions, anoxic/euxinic sediments can lack a Mo-enrichment.

For the EEBS, widespread anoxic–euxinic conditions occur in the T-CIE interval marking the peak T-OAE (e.g., Röhl et al. 2001; Schwark and Frimmel 2004; McArthur et al. 2008; Burnaz et al. 2024) and were confirmed for the Hondelage succession in this study. Sediments corresponding to the Jenkyns Event are characterized by low to moderate Mo-enrichment, which has been interpreted to reflect the Mo drawdown in the restricted EEBS under prolonged euxinic conditions (e.g., McArthur et al. 2008). A comparable pattern was observed at Hondelage with lowest Mo_{EF} seen in samples from the Pliensbachian (interval 1) explained by a well-oxygenated depositional setting in which Mo is not efficiently transferred from the water column to the sediment. Sediments of the Toarcian Interval II show a significant enrichment in TOC, Cu, and U, while only minor enrichments are seen in V and Mo. This pattern attests to rather suboxic-anoxic conditions that favored organic matter preservation, but not the enrichment of elements with euxinic affinity, such as V and Mo (Algeo and Maynard 2004). High Mo_{EF} are seen in interval III that corresponds to the core of the T-CIE, for which prolonged euxinic conditions have been inferred. Throughout the intervals IV–VI, Mo_{EF} mainly follows trends seen in the enrichment of V, indicating that Mo-enrichment was controlled by changes in the redox conditions and replenishment through water mass renewal. Hence, the highest observed Mo concentrations in interval VI could be explained by increased water mass exchange.

The cross-plots of Mo versus TOC and U_{EF} versus Mo_{EF} attest to significant changes in the Mo burial in the anoxic–euxinic strata of the Posidonia Shale (intervals II–VI). In the cross-plot of TOC *vs.* Mo (Fig. 10a), samples from intervals II–IV plot below the Black Sea

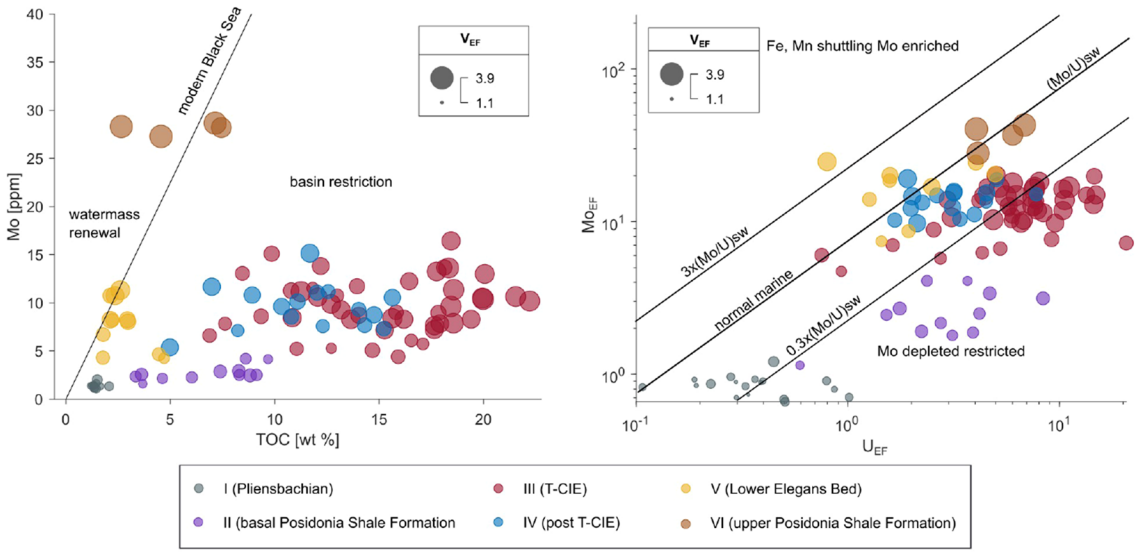

Fig. 10 Left: TOC (%) *vs.* Mo (ppm) with the black line indicating the modern Black Sea ratio (Algeo and Lyons 2006): Samples plotting below the Black Sea line indicate a more severe restriction than evident for the Black Sea. Right: Increases in the ratio indicate enhanced water mass enrichment of Mo (Mo_{EF}) *vs.* U (U_{EF}). Black lines represent the ratio of Mo/U in sea water under normal marine conditions, Mo-depleted (basin restriction) and Mo-enriched conditions (Fe, Mn shuttling) adapted from Algeo and Tribovillard (2009). The size of data symbols represents V_{EF}

trend, which characterizes highly restricted and Mo-depleted basins (Algeo and Lyons 2006). This pattern is in agreement with data from coeval strata that also lack a significant Mo-enrichment, although they were deposited under euxinic conditions (e.g., McArthur et al. 2008; Hermoso et al. 2013; Fernández-Martínez et al. 2023). For these intervals, the cross-plot of U_{EF} with Mo_{EF} indicates a rather low aqueous Mo inventory (Fig. 10b), which is best explained by the establishment of prolonged euxinia in a hydrologically restricted basin with limited water exchange with the open ocean. In addition, the global scale expansion of anoxic/euxinic sinks during the climax of the T-OAE (T-CIE interval) led to a decline in the Ocean Mo inventory (Dickson et al. 2017; Them et al. 2022).

An increase in the Mo_{EF} is seen in the post-Lower Elegans Bed interval VI (Fig. 5). A comparable pattern of increasing sedimentary Mo-enrichment is apparent in coeval strata form other basins and is best explained by a replenishment of Mo_{sw} via the enhanced connectivity of the EEBS with the Tethyan and Artic Oceans (McArthur et al. 2008). In post T-CIE intervals, increased Mo-enrichment in anoxic/euxinic basins may also be related to a replenishment of the global Ocean Mo inventory, due to an overall decline of anoxic/euxinic sinks (Dickson et al. 2017; Them et al. 2022).

Conclusion

Although the North-German Basin (NGB) has been studied for its depositional environment during the Pliensbachian/Toarcian transition before, comparably few studies exploiting the potential of complementary application of organic, elemental and isotope proxies embedded in a detailed biostratigraphic framework exist. The succession from Hondelage in the NGB covers the latest Pliensbachian to Early Toarcian interval including the Toarcian Carbon Isotope Excursion (T-CIE). Bio- and chemostratigraphic data suggest that the Pliensbachian Toarcian boundary and parts of the lower *D. tenuicostum* Zone are missing.

High-resolution geochemical data show that in the NGB changes in sedimentation, terrestrial input, redox conditions and organic matter accumulation are closely linked to sea-level fluctuations mediated by continental ice sheet volume and the climate-dependent hydrological cycle. The positive correlation of Zr/Al and TOC suggests fluvial input as main driver of soil-derived nutrient supply, which promoted high primary productivity during the Toarcian. This is supported by evidence for enhanced soil erosion leading to an increased input of refractory organic matter, as seen in the increased x-intercept of the regression line in a TOC *vs.* S2 cross-plot. In contrast, low marine productivity and poor organic matter preservation under oxic to suboxic conditions prevailed during the Pliensbachian. An enhanced hydrological cycle during the T-CIE counterintuitively led to a decreased chemical index of alteration,

presumably due to shorter residence times and faster transport of sediments from terrestrial sources to the marine basin. The source regions supplying sediment likely were proximal islands (Calvörde Island, Altmark Swell) as well as the Bohemian Massif hosting a large delta system with a sediment focusing toward the Oberaller Trough. The lowered sea level during the Pliensbachian coldhouse climate likely caused better bottom water ventilation with oxic to suboxic conditions and low accumulation of redox-sensitive trace elements. With increasing sea level, freshwater stratification, and export productivity, the oxygen levels decreased and anoxic to euxinic conditions established, reaching a maximum during the T-CIE. However, severe basin restriction prohibited further trace element enrichment in the sediments due to their drawdown in ocean waters. A sea-level drop toward the Lower Elegans Bed reduced anoxic conditions and coincided with increased carbonate precipitation, reduced terrestrial input and primary productivity, presumably due to reduced nutrient and freshwater input as well as a recovery of the carbonate factory. A presumed sea-level rise in uppermost part of the succession likely led to increased water mass exchange causing trace element replenishment leading to highest trace element abundances, coinciding with increased primary productivity and terrigenous nutrient supply.

Supplementary Information The online version contains supplementary material available at https://doi.org/10.1007/s00531-024-02433-7.

Acknowledgements Yves Brügger (University of Zurich) is acknowledged for great laboratory assistance. Marieke Muijsers and Fanny Aschmann are thanked for excellent laboratory assistance at Kiel University.

Funding Open Access funding enabled and organized by Projekt DEAL. Deutsche Forschungsgemeinschaft, Schw554/29-1, Lorenz Schwark

Data availability Data is available as supplementary information.

Declarations

Conflict of interests The authors declare that they have no known competing financial interests or personal relationships that could have influenced the work reported in this paper.

References

Ajuaba S, Sachsenhofer RF, Bechtel A, Galasso F, Gross D, Misch D, Schneebeli-Hermann E (2022) Biomarker and compound-specific isotope records across the Toarcian CIE at the Dormettingen section in SW Germany. Int J Earth Sci 111:1631–1661. https://doi.org/10.1007/s00531-022-02196-z

Algeo TJ, Lyons TW (2006) Mo–total organic carbon covariation in modern anoxic marine environments: Implications for analysis of paleoredox and paleohydrographic conditions. Paleoceanography. https://doi.org/10.1029/2004PA001112

Algeo TJ, Maynard J (2004) Trace-element behavior and redox facies in core shales of Upper Pennsylvanian Kansas-type cyclothems. Chem Geol 206(3–4):289–318. https://doi.org/10.1016/j.chemgeo.2003.12.009

Algeo TJ, Tribovillard N (2009) Environmental analysis of paleoceanographic systems based on molybdenum–uranium covariation. Chem Geol 268(3–4):211–225. https://doi.org/10.1016/j.chemgeo.2009.09.001

Arp G, Balmuk Y, Seppelt S, Reimer A (2023) Biostratigraphy and sedimentary sequences of the Toarcian Hainberg section (Northwestern Harz foreland, Northern Germany). Zitteliana 97:1–27. https://doi.org/10.3897/zitteliana.97.110677

Baghli H, Mattioli E, Spangenberg JE, Ruebsam W, Schwark L, Bensalah M, Sebane A, Pittet B, Pellenard P, Suan G (2022) Stratification and productivity in the Western Tethys (NW Algeria) during early Toarcian. Palaeogeogr Palaeoclimatol Palaeoecol 591:110864. https://doi.org/10.1016/j.palaeo.2022.110864

Barth G, Pieńkowski G, Zimmermann J, Franz M, Kuhlmann G (2018) Palaeogeographical evolution of the Lower Jurassic: high-resolution biostratigraphy and sequence stratigraphy in the Central European Basin. Geo Soc London Special Pub 469(1):341–369. https://doi.org/10.1144/SP469.8

Beerling DJ, Brentnall SJ (2007) Numerical evaluation of mechanisms driving Early Jurassic changes in global carbon cycling. Geology 35(3):247. https://doi.org/10.1130/G23416A.1

Berner RA, Raiswell R (1983) Burial of organic carbon and pyrite sulfur in sediments over phanerozoic time: a new theory. Geochim Cosmochim Acta 47(5):855–862. https://doi.org/10.1016/0016-7037(83)90151-5

Bianchi TS, Allison MA (2009) Large-river delta-front estuaries as natural "recorders" of global environmental change. Proc Natl Acad Sci USA 106(20):8085–8092. https://doi.org/10.1073/pnas.0812878106

Bodin S, Fantasia A, Krencker F-N, Nebsbjerg B, Christiansen L, Andrieu S (2023) More gaps than record! A new look at the Pliensbachian/Toarcian boundary event guided by coupled chemo-sequence stratigraphy. Palaeogeogr Palaeoclimatol Palaeoecol 610:111344. https://doi.org/10.1016/j.palaeo.2022.111344

Bordenave ML, Espitalié J, Leplat P, Oudin JL, Vandenbroucke M (1993) Screening techniques for source rock evaluation. Applied Petroleum Geochemistry. https://doi.org/10.12691/jgg-4-4-2

Brazier J-M, Suan G, Tacail T, Simon L, Martin JE, Mattioli E, Balter V (2015) Calcium isotope evidence for dramatic increase of continental weathering during the Toarcian oceanic anoxic event (Early Jurassic). Earth Planet Sci Lett 411:164–176. https://doi.org/10.1016/j.epsl.2014.11.028

Brumsack H-J (1991) Inorganic geochemistry of the German 'Posidonia Shale': palaeoenvironmental consequences. In: TYSON RV & PEARSON TH (eds) Modern and Ancient Continental Shelf Anoxia. Geological Society Special Publication. https://doi.org/10.1144/GSL.SP.1991.058.01.22

Burnaz L, Littke R, Grohmann S, Erbacher J, Strauss H, Amann F. (2024). Lower Jurassic Pliensbachian–Toarcian marine

paleoenvironment in Western Europe sedimentology, geochemistry and organic petrology of the wells Mainzholzen and Wickensen, Hils Syncline Lower Saxony Basin. International Journal of Earth Sciences. https://doi.org/10.1007/s00531-023-02381-8

Cohen AS, Coe AL, Harding SM, Schwark L (2004) Osmium isotope evidence for the regulation of atmospheric CO2 by continental weathering. Geology 32(2):157. https://doi.org/10.1130/G20158.1

Danise S, Twitchett RJ, Little CT (2015) Environmental controls on Jurassic marine ecosystems during global warming. Geology 43(3):263–266. https://doi.org/10.1130/G36390.1

Delaney ML (1998) Phosphorus accumulation in marine sediments and the oceanic phosphorus cycle. Global Biogeochem Cycles 12(4):563–572. https://doi.org/10.1029/98GB02263

Dera G, Pellenard P, Neige P, Deconinck J-F, Pucéat E, Dommergues J-L (2009) Distribution of clay minerals in Early Jurassic Peritethyan seas: Palaeoclimatic significance inferred from multiproxy comparisons. Palaeogeogr Palaeoclimatol Palaeoecol 271(1–2):39–51. https://doi.org/10.1016/j.palaeo.2008.09.010

Dickson AJ, Gill BC, Ruhl M, Jenkyns HC, Porcelli D, Idiz E, Lyons TW, Boorn SHJM (2017) Molybdenum-isotope chemostratigraphy and paleoceanography of the Toarcian Oceanic Anoxic Event (Early Jurassic). Paleoceanography 32(8):813–829. https://doi.org/10.1002/2016PA003048

Dypvik H, Harris NB (2001) Geochemical facies analysis of fine-grained siliciclastics using Th/U, Zr/Rb and (Zr+Rb)/Sr ratios. Chem Geol 181(1–4):131–146. https://doi.org/10.1016/S0009-2541(01)00278-9

Emerson SR, Huested SS (1991) Ocean anoxia and the concentrations of molybdenum and vanadium in seawater. Mar Chem 34(3–4):177–196. https://doi.org/10.1016/0304-4203(91)90002-E

Espitalie J, Deroo G, Marquis F (1985). La Pyrolyse Rock-Eval Et Ses Applications Revue De L'institut Français Du Pétrole Deuxième Partie. https://doi.org/10.2516/ogst:1985045

Fantasia A, Adatte T, Spangenberg JE, Font E, Lv D, Föllmi KB (2019) Global versus local processes during the Pliensbachian-Toarcian transition at the Peniche GSSP, Portugal: A multi-proxy record. Earth Sci Rev 198:102932. https://doi.org/10.1016/j.earscirev.2019.102932

Fernández-Martínez J, Ruíz FM, Rodríguez-Tovar FJ, Piñuela L, García-Ramos JC, Algeo TJ (2023) Euxinia and hydrographic restriction in the Tethys Ocean: Reassessing global oceanic anoxia during the early Toarcian. Global Planet Change 221:104026. https://doi.org/10.1016/j.gloplacha.2022.104026

Frimmel A, Oschmann W, Schwark L (2004) Chemostratigraphy of the Posidonia Black Shale. SW Germany Chemical Geology 206(3–4):199–230. https://doi.org/10.1016/j.chemgeo.2003.12.007

Gambacorta G, Brumsack H-J, Jenkyns HC, Erba E (2024) The early Toarcian Oceanic Anoxic Event (Jenkyns Event) in the Alpine-Mediterranean Tethys, north African margin, and north European epicontinental seaway. Earth Sci Rev 248:104636. https://doi.org/10.1016/j.earscirev.2023.104636

Ganeshram RS, Calvert SE, Pedersen TF, Cowie GL (1999) Factors controlling the burial of organic carbon in laminated and bioturbated sediments off NW Mexico: implications for hydrocarbon preservation. Geochim Cosmochim Acta 63(11–12):1723–1734. https://doi.org/10.1016/S0016-7037(99)00073-3

Govin A, Holzwarth U, Heslop D, Ford Keeling L, Zabel M, Mulitza S, Collins JA, Chiessi CM (2012) Distribution of major elements in Atlantic surface sediments (36°N–49°S): Imprint of terrigenous input and continental weathering. Geochem Geophys Geosyst. https://doi.org/10.1029/2011GC003785

Gröcke DR. (2020). Carbon isotope stratigraphy: Principles and applications. In: Carbon Isotope Stratigraphy, Elsevier,

Hallam A (1997) Estimates of the amount and rate of sea-level change across the Rhaetian—Hettangian and Pliensbachian—Toarcian boundaries (latest Triassic to early Jurassic). J Geol Soc 154(5):773–779. https://doi.org/10.1144/gsjgs.154.5.0773

Harries PJ, Little CT (1999) The early Toarcian (Early Jurassic) and the Cenomanian-Turonian (Late Cretaceous) mass extinctions: similarities and contrasts. Palaeogeogr Palaeoclimatol Palaeoecol 154(1–2):39–66. https://doi.org/10.1016/S0031-0182(99)00086-3

Helz GR, Miller CV, Charnock JM, Mosselmans J, Pattrick R, Garner CD, Vaughan DJ (1996) Mechanism of molybdenum removal from the sea and its concentration in black shales: EXAFS evidence. Geochim Cosmochim Acta 60(19):3631–3642. https://doi.org/10.1016/0016-7037(96)00195-0

Hermoso M, Le Callonnec L, Minoletti F, Renard M, Hesselbo SP (2009) Expression of the Early Toarcian negative carbon-isotope excursion in separated carbonate microfractions (Jurassic, Paris Basin). Earth Planet Sci Lett 277(1–2):194–203. https://doi.org/10.1016/j.epsl.2008.10.013

Hermoso M, Minoletti F, Pellenard P (2013) Black shale deposition during Toarcian super-greenhouse driven by sea level. Climate of the past 9(6):2703–2712. https://doi.org/10.5194/cp-9-2703-2013

Hesselbo SP, Gröcke DR, Jenkyns HC, Bjerrum CJ, Farrimond P, Morgans Bell HS, Green OR (2000) Massive dissociation of gas hydrate during a Jurassic oceanic anoxic event. Nature 406(6794):392–395. https://doi.org/10.1038/35019044

Hesselbo SP, Jenkyns HC, Duarte LV, Oliveira LC (2007) Carbon-isotope record of the Early Jurassic (Toarcian) Oceanic Anoxic Event from fossil wood and marine carbonate (Lusitanian Basin, Portugal). Earth Planet Sci Lett 253(3–4):455–470. https://doi.org/10.1016/j.epsl.2006.11.009

Hoffmann K (1966) Die Stratigraphie und Paläogeographie der bituminösen Fazies des nordwestdeutschen Oberlias (Toarcium). Beihefte Geologisches Jahrbuch 58:443–498

Hoffmann K (1968) Neue Ammonitenfunde aus dem tieferen Unter-Toarcium (Lias epsilon) des nördlichen Harzvorlandes und ihre feinstratigraphische Bedeutung. Geologisches Jahrbuch(85):1–32

Ingall ED, Bustin RM, van Cappellen P (1993) Influence of water column anoxia on the burial and preservation of carbon and phosphorus in marine shales. Geochim Cosmochim Acta 57(2):303–316. https://doi.org/10.1016/0016-7037(93)90433-W

Izumi K, Kemp DB, Itamiya S, Inui M (2018) Sedimentary evidence for enhanced hydrological cycling in response to rapid carbon release during the early Toarcian oceanic anoxic event. Earth Planet Sci Lett 481:162–170. https://doi.org/10.1016/j.epsl.2017.10.030

Jarvis I, Burnett WC, Nathan Y, Almbaydin FS, Attia AK, Castro LN, Flicoteaux R, Hilmy ME, Husain V, Qutawnah AA (1994) Phosphorite geochemistry: state-of-the-art and environmental concerns. Eclogae Geol Helv 87(3):643–700

Jenkyns HC (1985) The early Toarcian and Cenomanian-Turonian anoxic events in Europe: comparisons and contrasts. Geol Rundsch 74(3):505–518. https://doi.org/10.1007/BF01821208

Jenkyns HC (1988) The early Toarcian (Jurassic) anoxic event; stratigraphic, sedimentary and geochemical evidence. Am J Sci 288(2):101–151. https://doi.org/10.2475/ajs.288.2.101

Jenkyns HC (2010) Geochemistry of oceanic anoxic events. Geochem Geophys Geosyst. https://doi.org/10.1029/2009GC002788

Jenkyns HC, Clayton CJ (1986) Black shales and carbon isotopes in pelagic sediments from the Tethyan Lower Jurassic. Sedimentology 33(1):87–106. https://doi.org/10.1111/j.1365-3091.1986.tb00746.x

Jenkyns HC, Clayton CJ (1997) Lower Jurassic epicontinental carbonates and mudstones from England and Wales: chemostratigraphic signals and the early Toarcian anoxic event. Sedimentology 44(4):687–706. https://doi.org/10.1046/j.1365-3091.1997.d01-43.x

Kaplan ME (1978) Calcite pseudomorphoses in Jurassic and Lower Cretaceous deposits of the northern area of eastern Siberia. Geol Geofiz 19:62–70

Kemp DB, Coe AL, Cohen AS, Schwark L (2005) Astronomical pacing of methane release in the Early Jurassic period. Nature 437(7057):396–399. https://doi.org/10.1038/nature04037

Kemp DB, Selby D, Izumi K (2020) Direct coupling between carbon release and weathering during the Toarcian oceanic anoxic event. Geology 48(10):976–980. https://doi.org/10.1130/G47509.1

Kemp DB, Chen W, Cho T, Algeo TJ, Shen J, Ikeda M (2022) Deep-ocean anoxia across the Pliensbachian-Toarcian boundary and the Toarcian Oceanic Anoxic Event in the Panthalassic Ocean. Global Planet Change 212:103782. https://doi.org/10.1016/j.gloplacha.2022.103782

Klopschar M (2006) Hondelage: Grube im Posidonienschiefer (Lias epsilon). Bruanschweiger Land - Wanderungen in die Erdgeschichte:119–124

Korte C, Hesselbo SP, Ullmann CV, Dietl G, Ruhl M, Schweigert G, Thibault N (2015) Jurassic climate mode governed by ocean gateway. Nat Commun 6:10015. https://doi.org/10.1038/ncomms10015

Korty RL, Emanuel KA, Scott JR (2008) Tropical Cyclone-Induced Upper-Ocean Mixing and Climate: Application to Equable Climates. J Clim 21(4):638–654. https://doi.org/10.1175/2007JCLI1659.1

Krencker F-N, Bodin S, Suan G, Heimhofer U, Kabiri L, Immenhauser A (2015) Toarcian extreme warmth led to tropical cyclone intensification. Earth Planet Sci Lett 425:120–130. https://doi.org/10.1016/j.epsl.2015.06.003

Krencker F-N, Lindström S, Bodin S (2019) A major sea-level drop briefly precedes the Toarcian oceanic anoxic event: implication for Early Jurassic climate and carbon cycle. Sci Rep 9(1):12518. https://doi.org/10.1038/s41598-019-48956-x

Krencker F-N, Fantasia A, Danisch J, Martindale R, Kabiri L, El Ouali M, Bodin S (2020) Two-phased collapse of the shallow-water carbonate factory during the late Pliensbachian-Toarcian driven by changing climate and enhanced continental weathering in the Northwestern Gondwana Margin. Earth Sci Rev 208:103254. https://doi.org/10.1016/j.earscirev.2020.103254

Krencker F-N, Fantasia A, El Ouali M, Kabiri L, Bodin S (2022) The effects of strong sediment-supply variability on the sequence stratigraphic architecture: Insights from early Toarcian carbonate factory collapses. Mar Pet Geol 136:105469. https://doi.org/10.1016/j.marpetgeo.2021.105469

Littke R, Klussmann U, Krooss B, Leythaeuser D (1991a) Quantification of loss of calcite, pyrite, and organic matter due to weathering of Toarcian black shales and effects on kerogen and bitumen characteristics. Geochim Cosmochim Acta 55(11):3369–3378. https://doi.org/10.1016/0016-7037(91)90494-p

Littke R, Leythaeuser D, Rullkötter J, Baker DR (1991b) Keys to the depositional history of the Posidonia Shale (Toarcian) in the Hils Syncline, northern Germany. Geological Society, London, Special Publications 58(1):311–333. https://doi.org/10.1144/GSL.SP.1991.058.01.20

Little CTS, Benton MJ (1995) Early Jurassic mass extinction: A global long-term event. Geology 23(6):495. https://doi.org/10.1130/0091-7613(1995)023%3c0495:EJMEAG%3e2.3.CO;2

Loh H, Maul B, Prauss M, Riegel W (1986) Primary production, maceral formation and carbonate species in the Posidonia Shale of NW Germany. Mitteilung der Geologisch-Palaontologischen Institut der Universitat Hamburg

Marynowski L, Pisarzowska A, Derkowski A, Rakociński M, Szaniawski R, Środoń J, Cohen AS (2017) Influence of palaeoweathering on trace metal concentrations and environmental proxies in black shales. Palaeogeogr Palaeoclimatol Palaeoecol 472:177–191. https://doi.org/10.1016/j.palaeo.2017.02.023

Mattioli E, Pittet B (2002) Contribution of calcareous nannoplankton to carbonate deposition: a new approach applied to the Lower Jurassic of central Italy. Mar Micropaleontol 45(2):175–190. https://doi.org/10.1016/S0377-8398(02)00039-7

Mattioli E, Pittet B (2004) Spatial and temporal distribution of calcareous nannofossils along a proximal–distal transect in the Lower Jurassic of the Umbria–Marche Basin (central Italy). Palaeogeogr Palaeoclimatol Palaeoecol 205(3–4):295–316. https://doi.org/10.1016/j.palaeo.2003.12.013

Mattioli E, Pittet B, Suan G, Mailliot S (2008) Calcareous nannoplankton changes across the early Toarcian oceanic anoxic event in the western Tethys. Paleoceanography. https://doi.org/10.1029/2007PA001435

Mattioli E, Pittet B, Petitpierre L, Mailliot S (2009) Dramatic decrease of pelagic carbonate production by nannoplankton across the Early Toarcian anoxic event (T-OAE). Global Planet Change 65(3–4):134–145. https://doi.org/10.1016/j.gloplacha.2008.10.018

McArthur JM, Algeo TJ, van de Schootbrugge B, Li Q, Howarth RJ (2008) Basinal restriction, black shales, Re-Os dating, and the Early Toarcian (Jurassic) oceanic anoxic event. Paleoceanography. https://doi.org/10.1029/2008PA001607

Merkel A, Munnecke A (2023) Glendonite-bearing concretions from the upper Pliensbachian (Lower Jurassic) of South Germany: indicators for a massive cooling in the European epicontinental sea. Facies. https://doi.org/10.1007/s10347-023-00667-6

Montero-Serrano J-C, Föllmi KB, Adatte T, Spangenberg JE, Tribovillard N, Fantasia A, Suan G (2015) Continental weathering and redox conditions during the early Toarcian Oceanic Anoxic Event in the northwestern Tethys: Insight from the Posidonia Shale section in the Swiss Jura Mountains. Palaeogeogr Palaeoclimatol Palaeoecol 429:83–99. https://doi.org/10.1016/j.palaeo.2015.03.043

Morard A, Guex J, Bartolini A, Morettini E, de Wever P (2003) A new scenario for the Domerian - Toarcian transition. Bulletin De La Société Géologique De France 174(4):351–356. https://doi.org/10.2113/174.4.351

Müller T, Price GD, Bajnai D, Nyerges A, Kesjár D, Raucsik B, Varga A, Judik K, Fekete J, May Z, Pálfy J (2017) New multiproxy record of the Jenkyns Event (also known as the Toarcian Oceanic Anoxic Event) from the Mecsek Mountains (Hungary): Differences, duration and drivers. Sedimentology 64(1):66–86. https://doi.org/10.1111/sed.12332

Mutterlose J, Klopschar M, Visentin S (2022) Ecological adaptation of marine floras and faunas across the Early Jurassic Toarcian Oceanic Anoxic Event – A case study from northern Germany. Palaeogeogr Palaeoclimatol Palaeoecol 602:111176. https://doi.org/10.1016/j.palaeo.2022.111176

Nesbitt HW, Young GM (1982) Early Proterozoic climates and plate motions inferred from major element chemistry of lutites. Nature 299(5885):715–717. https://doi.org/10.1038/299715a0

Ott S (1967) Beitrag zur Kenntnis der stratigraphischen paläogeographischen und tektonischen Verhältnisse der östlichen Subherzynen Kreidemulde, Ernst-Moritz-Arndt-Universität Greifswald

Page KN (2003) The Lower Jurassic of Europe: its subdivision and correlation. GEUS Bulletin 1:21–59

Percival L, Witt M, Mather TA, Hermoso M, Jenkyns HC, Hesselbo SP, Al-Suwaidi AH, Storm MS, Xu W, Ruhl M (2015) Globally enhanced mercury deposition during the end-Pliensbachian extinction and Toarcian OAE: A link to the Karoo-Ferrar Large Igneous Province. Earth Planet Sci Lett 428:267–280. https://doi.org/10.1016/j.epsl.2015.06.064

Perkins RB, Mason CE (2015) The relative mobility of trace elements from short-term weathering of a black shale. Appl Geochem 56:67–79. https://doi.org/10.1016/j.apgeochem.2015.01.014

Pittet B, Suan G, Lenoir F, Duarte LV, Mattioli E (2014) Carbon isotope evidence for sedimentary discontinuities in the lower Toarcian of the Lusitanian Basin (Portugal): Sea level change at the onset of the Oceanic Anoxic Event. Sed Geol 303:1–14. https://doi.org/10.1016/j.sedgeo.2014.01.001

Prauss M, Ligouis B, Luterbacher H (1991) Organic matter and palynomorphs in the 'Posidonienschiefer' (Toarcian, Lower Jurassic) of southern Germany. Geological Society, London, Special Publications 58(1):335–351. https://doi.org/10.1144/GSL.SP.1991.058.01.21

Prauss M (1996) The Lower Toarcian Posidonia Shale of Grimmen, Northeast Germany. Implications from the palynological analysis of a near-shore section. Neues Jahrbuch für Geologie und Paläontologie-Abhandlungen:107–132

Redfield AC (1958) The biological control of chemical factors in the environment. Am Sci 46(3):230A-A221

Reimers CE, Ruttenberg KC, Canfield DE, Christiansen MB, Martin JB (1996) Porewater pH and authigenic phases formed in the uppermost sediments of the Santa Barbara Basin. Geochim Cosmochim Acta 60(21):4037–4057. https://doi.org/10.1016/S0016-7037(96)00231-1

Reolid M, Rodriguez-Tovar FJ, Marok A, Sebane A (2012) The Toarcian oceanic anoxic event in the Western Saharan Atlas, Algeria (North African paleomargin): Role of anoxia and productivity. Geol Soc Am Bull 124(9–10):1646–1664. https://doi.org/10.1130/B30585.1

Reolid M, Chakiri S, Bejjaji Z (2013) Adaptative strategies of the Toarcian benthic foraminiferal assemblages from the Middle Atlas (Morocco): Palaeoecological implications. J Afr Earth Sc 84:1–12. https://doi.org/10.1016/j.jafrearsci.2013.03.008

Reolid M, Molina JM, Nieto LM, Rodríguez-Tovar FJ (2018) The Toarcian Oceanic Anoxic Event in the South Iberian Palaeomargin. Springer

Ricken W (1993) Sedimentation as a three-component system: organic carbon, carbonate, noncarbonate. Lecture Notes in Earth Sciences (51)

Riegel W, Loh H, Maul B, Prauss M (1986) Effects and causes in a black shale event: The Toarcian Posidonia Shale of NW Germany. Lecture Notes in Earth Sciences 1986(Vol. 8)

Röhl H-J, Schmid-Röhl A, Oschmann W, Frimmel A, Schwark L (2001) The Posidonia Shale (Lower Toarcian) of SW-Germany: an oxygen-depleted ecosystem controlled by sea level and palaeoclimate. Palaeogeogr Palaeoclimatol Palaeoecol 165(1–2):27–52. https://doi.org/10.1016/s0031-0182(00)00152-8

Ruebsam W, Al-Husseini M (2020) Calibrating the Early Toarcian (Early Jurassic) with stratigraphic black holes (SBH). Gondwana Res 82:317–336. https://doi.org/10.1016/j.gr.2020.01.011

Ruebsam W, Al-Husseini M (2021) Orbitally synchronized late Pliensbachian–early Toarcian glacio-eustatic and carbon-isotope cycles. Palaeogeogr Palaeoclimatol Palaeoecol 577:110562. https://doi.org/10.1016/j.palaeo.2021.110562

Ruebsam W, Schwark L (2021) Impact of a northern-hemispherical cryosphere on late Pliensbachian–early Toarcian climate and environment evolution. Geological Society, London, Special Publications 514(1):359–385. https://doi.org/10.1144/SP514-2021-11

Ruebsam W, Schwark L (2024) Disparity between Toarcian Oceanic Anoxic Event and Toarcian carbon isotope excursion. Int J Earth Sci. https://doi.org/10.1007/s00531-024-02408-

Ruebsam W, Müller T, Kovács J, Pálfy J, Schwark L (2018) Environmental response to the early Toarcian carbon cycle and climate perturbations in the northeastern part of the West Tethys shelf. Gondwana Res 59:144–158. https://doi.org/10.1016/j.gr.2018.03.013

Ruebsam W, Mayer B, Schwark L (2019) Cryosphere carbon dynamics control early Toarcian global warming and sea level evolution. Global Planet Change 172:440–453. https://doi.org/10.1016/j.gloplacha.2018.11.003

Ruebsam W, Reolid M, Sabatino N, Masetti D, Schwark L (2020a) Molecular paleothermometry of the early Toarcian climate perturbation. Global Planet Change 195:103351. https://doi.org/10.1016/j.gloplacha.2020.103351

Ruebsam W, Pieńkowski G, Schwark L (2020c) Toarcian climate and carbon cycle perturbations – its impact on sea-level changes, enhanced mobilization and oxidation of fossil organic matter. Earth Planet Sci Lett 546:116417. https://doi.org/10.1016/j.epsl.2020.116417

Ruebsam W, Reolid M, Mattioli E, Schwark L (2022a) Organic carbon accumulation at the northern Gondwana paleomargin (Tunisia) during the Toarcian Oceanic Anoxic Event: Sedimentological and geochemical evidence. Palaeogeogr Palaeoclimatol Palaeoecol 586:110781. https://doi.org/10.1016/j.palaeo.2021.110781

Ruebsam W, Mattioli E, Schwark L (2022b) Weakening of the biological pump induced by a biocalcification crisis during the early Toarcian Oceanic Anoxic Event. Global Planet Change 217:103954. https://doi.org/10.1016/j.gloplacha.2022.103954

Ruebsam W, Mattioli E, Schwark L (2022c) Molecular fossils and calcareous nannofossils reveal recurrent phytoplanktonic events in the early Toarcian. Global Planet Change 212:103812. https://doi.org/10.1016/j.gloplacha.2022.103812

Ruebsam W, Franz M, Ansorge J, Obst K, Schwark L (2024) Late Triassic to Early Jurassic carbon isotope chemostratigraphy and organo-facies evolution in a distal to proximal transect of the North German Basin. Int J Earth Sci. https://doi.org/10.1007/s00531-024-02418-6

Ruebsam W, Thibault N, Al-Husseini M (2020b) Early Toarcian glacio-eustatic unconformities and chemostratigraphic black holes. In: Carbon Isotope Stratigraphy, vol 5. Elsevier, pp 629–676

Rullkötter J, Leythaeuser D, Horsfield B, Littke R, Mann U, Müller P, Radke M, Schaefer R, Schenk H-J, Schwochau K, Witte E, Welte D (1988) Organic matter maturation under the influence of a deep intrusive heat source: A natural experiment for quantitation of hydrocarbon generation and expulsion from a petroleum source rock (Toarcian shale, northern Germany). Org Geochem 13(4–6):847–856. https://doi.org/10.1016/0146-6380(88)90237-9

Ruvalcaba Baroni I, Pohl A, van Helmond NAGM, Papadomanolaki NM, Coe AL, Cohen AS, van de Schootbrugge B, Donnadieu Y, Slomp CP (2018) Ocean Circulation in the Toarcian (Early Jurassic): A Key Control on Deoxygenation and Carbon Burial on the European Shelf. Paleoceanography and Paleoclimatology 33(9):994–1012. https://doi.org/10.1029/2018PA003394

Saelen G, Doyle P, Talbot MR (1996) Stable-Isotope Analyses of Belemnite Rostra from the Whitby Mudstone Fm. PALAIOS, England Surface Water Conditions during Deposition of a Marine Black Shale. https://doi.org/10.2307/3515065

Savrda CE, Bottjer DJ (1986) Trace-fossil model for reconstruction of paleo-oxygenation in bottom waters. Geology 14(1):3. https://doi.org/10.1130/0091-7613

Schwark L, Frimmel A (2004) Chemostratigraphy of the Posidonia Black Shale. SW-Germany Chem Geo 206(3–4):231–248. https://doi.org/10.1016/j.chemgeo.2003.12.008

Schwark L, Ruebsam W (2024) Climate cyclicity-controlled recurrent bottom-water ventilation events in the aftermath of the Toarcian Oceanic Anoxic Event: the Jenkyns Event. Int J Earth Sci. https://doi.org/10.1007/s00531-024-02417-7

Slater SM, Twitchett RJ, Danise S, Vajda V (2019) Substantial vegetation response to Early Jurassic global warming with impacts on oceanic anoxia. Nat Geosci 12:462–467. https://doi.org/10.1038/s41561-019-0349-z

Song J, Littke R, Weniger P (2017) Organic geochemistry of the Lower Toarcian Posidonia Shale in NW Europe. Org Geochem 106:76–92. https://doi.org/10.1016/j.orggeochem.2016.10.014

Stock AT, Littke R, Schwarzbauer J, Horsfield B, Hartkopf-Fröder C (2017) Organic geochemistry and petrology of Posidonia Shale (Lower Toarcian, Western Europe) – The evolution from immature oil-prone to overmature dry gas-producing kerogen. Int J Coal Geol 176–177:36–48. https://doi.org/10.1016/j.coal.2017.04.016

Suan G, Mattioli E, Pittet B, Lécuyer C, Suchéras-Marx B, Duarte LV, Philippe M, Reggiani L, Martineau F (2010) Secular environmental precursors to Early Toarcian (Jurassic) extreme climate changes. Earth Planet Sci Lett 290(3–4):448–458. https://doi.org/10.1016/j.epsl.2009.12.047

Suan G, Nikitenko BL, Rogov MA, Baudin F, Spangenberg JE, Knyazev VG, Glinskikh LA, Goryacheva AA, Adatte T, Riding JB, Föllmi KB, Pittet B, Mattioli E, Lécuyer C (2011) Polar record of Early Jurassic massive carbon injection. Earth Planet Sci Lett 312(1–2):102–113. https://doi.org/10.1016/j.epsl.2011.09.050

Svensen H, Planke S, Chevallier L, Malthe-Sørenssen A, Corfu F, Jamtveit B (2007) Hydrothermal venting of greenhouse gases triggering Early Jurassic global warming. Earth Planet Sci Lett 256(3–4):554–566. https://doi.org/10.1016/j.epsl.2007.02.013

Taylor SR, McLennan SM (1985) The continental crust: Its composition and evolution. Blackwell Scientific Publications, Palo Alto, CA

Teichert B, Luppold FW (2013) Glendonites from an Early Jurassic methane seep — Climate or methane indicators? Palaeogeogr Palaeoclimatol Palaeoecol 390:81–93. https://doi.org/10.1016/j.palaeo.2013.03.001

Them TR, Gill BC, Selby D, Gröcke DR, Friedman RM, Owens JD (2017) Evidence for rapid weathering response to climatic warming during the Toarcian Oceanic Anoxic Event. Sci Rep 7(1):5003. https://doi.org/10.1038/s41598-017-05307-y

Them TR, Owens JD, Marroquín SM, Caruthers AH, Alexandre JPT, Gill BC (2022) Reduced Marine Molybdenum Inventory Related to Enhanced Organic Carbon Burial and an Expansion of Reducing Environments in the Toarcian (Early Jurassic) Oceans. AGU Advances. https://doi.org/10.1029/2022AV000671

Thibault N, Ruhl M, Ullmann CV, Korte C, Kemp DB, Gröcke DR, Hesselbo SP (2018) The wider context of the Lower Jurassic Toarcian oceanic anoxic event in Yorkshire coastal outcrops. UK Proceedings of the Geologists' Association 129(3):372–391. https://doi.org/10.1016/j.pgeola.2017.10.007

Tribovillard N, Algeo TJ, Lyons T, Riboulleau A (2006) Trace metals as paleoredox and paleoproductivity proxies: An update. Chem Geol 232(1–2):12–32. https://doi.org/10.1016/j.chemgeo.2006.02.012

Tyson RV, Pearson TH (1991) Modern and ancient continental shelf anoxia: an overview. Geological Society London,special Publications 58(1):1–24. https://doi.org/10.1144/GSL.SP.1991.058.01.01

van Cappellen P, Ingall ED (1994) Benthic phosphorus regeneration, net primary production, and ocean anoxia: a model of the coupled marine biogeochemical cycles of carbon and phosphorus. Paleoceanography 9(5):677–692. https://doi.org/10.1029/94PA01455

van Breugel Y, Baas M, Schouten S, Mattioli E, Sinninghe Damsté JS (2006) Isorenieratane record in black shales from the Paris Basin, France: Constraints on recycling of respired CO 2 as a mechanism for negative carbon isotope shifts during the Toarcian oceanic anoxic event. Paleoceanography. https://doi.org/10.1029/2006PA001305

van Helmond NAGM, Sluijs A, Sinninghe Damsté JS, Reichart G-J, Voigt S, Erbacher J, Pross J, Brinkhuis H (2015) Freshwater discharge controlled deposition of Cenomanian-Turonian black shales on the NW European epicontinental shelf (Wunstorf, northern Germany). Climate past 11(3):495–508. https://doi.org/10.5194/cp-11-495-2015

van Hinsbergen DJJ, de Groot LV, van Schaik SJ, Spakman W, Bijl PK, Sluijs A, Langereis CG, Brinkhuis H (2015) A paleolatitude calculator for paleoclimate studies. PLoS ONE 10(6):e0126946. https://doi.org/10.1371/journal.pone.0126946

van de Schootbrugge B, Richoz S, Pross J, Luppold FW, Hunze S, Wonik T, Blau J, Meister C, van der Weijst C, Suan G, Fraguas A, Fiebig J, Herrle JO, Guex J, Little C, Wignall PB, Püttmann W, Oschmann W (2019) The Schandelah Scientific Drilling Project: A 25-million year record of Early Jurassic palaeo-environmental change from northern Germany. Newsletter Stratigraphy 52(3):249–296. https://doi.org/10.1127/nos/2018/0259

Visentin S, Erba E (2021) High-Resolution Calcareous Nannofossil Biostratigraphy across the Toarcian Oceanic Anoxic Event in Northern Italy: Clues from the Sogno and Gajum Cores (Lombardy Basin, Southerrn Alps). Riv Ital Paleontol Stratigr 127(3):2021. https://doi.org/10.13130/2039-4942/16313

Visentin S, Erba E, Mutterlose J (2022) Bio- and Chemostratigraphy of the Posidonia Shale: a New Database for the Toarcian Oceanic Anoxic Event from Northern Germany. Newsletters Stratigraphy. https://doi.org/10.1127/nos/2021/0658

Wignall PB (1991) Model for transgressive black shales? Geology 19(2):167. https://doi.org/10.1130/0091-7613

Wignall PB (2005) The timing of paleoenvironmental change and cause-and-effect relationships during the early Jurassic mass extinction in Europe. Am J Sci 305(10):1014–1032. https://doi.org/10.2475/ajs.305.10.1014

Wunnenberg C (1927) Beiträge zur Kenntnis des Lias in der Umgebung Braunschweigs. Jahrbuch Des Verbandes Naturwissenschaftler Braunschweig 20:56–80

Xu W, Ruhl M, Jenkyns HC, Leng MJ, Huggett JM, Minisini D, Ullmann CV, Riding JB, Weijers JW, Storm MS, Percival LM, Tosca NJ, Idiz EF, Tegelaar EW, Hesselbo SP (2018) Evolution of the Toarcian (Early Jurassic) carbon-cycle and global climatic controls on local sedimentary processes (Cardigan Bay Basin, UK). Earth Planet Sci Lett 484:396–411. https://doi.org/10.1016/j.epsl.2017.12.037

Ziegler PA (1990) Geological atlas of Western and Central Europe, 2nd and completely, rev. Shell Internationale Petroleum Maatschappij, The Hague

Zimmermann J, Franz M, Schaller A, Wolfgramm M (2018) The Toarcian-Bajocian deltaic system in the North German Basin: Subsurface mapping of ancient deltas-morphology, evolution and controls. Sedimentology 65(3):897–930. https://doi.org/10.1111/sed.12410